ADVANCED MATERIALS

Supporting Information

for *Adv. Mater.*, DOI 10.1002/adma.202307402

High-Performance Organic Electrochemical Transistors Achieved by Optimizing Structural and Energetic Ordering of Diketopyrrolopyrrole-Based Polymers

Il-Young Jo, Dahyun Jeong, Yina Moon, Dongchan Lee, Seungjin Lee, Jun-Gyu Choi, Donghyeon Nam, Ji Hwan Kim, Jinhan Cho, Shinuk Cho, Dong-Yu Kim, HyungJu Ahn, Bumjoon J. Kim and Myung-Han Yoon**

Supporting Information

High- Performance Organic Electrochemical Transistors Achieved by Optimizing Structural and Energetic Ordering of Diketopyrrolopyrrole-based Polymers

Il-Young Jo,† Dahyun Jeong,† Yina Moon, Dongchan Lee, Seungjin Lee, Jun-Gyu Choi, Donghyeon Nam, Ji Hwan Kim, Jinhan Cho, Shinuk Cho, Dong-Yu Kim, HyungJu Ahn, Bumjoon J. Kim, and Myung-Han Yoon**

I.-Y. Jo, Y. Moon, J.-G. Choi, J. H. Kim, Prof. D.-Y. Kim, Prof. M.-H. Yoon
School of Materials Science and Engineering
Gwangju Institute of Science and Technology (GIST)
Gwangju 61005, Republic of Korea
E-mail: mhyoon@gist.ac.kr

D. Jeong, S. Lee, Prof. B. J. Kim
Department of Chemical and Biomolecular Engineering
Korea Advanced Institute of Science and Technology (KAIST)
Daejeon 34141, Republic of Korea
E-mail: bumjoonkim@kaist.ac.kr

D. Lee, Prof. S. Cho
Department of Physics and EHSRC
University of Ulsan
Ulsan 44610, Republic of Korea

D. Nam, Prof. J. Cho
Department of Chemical and Biological Engineering
Korea University
Seoul 02841, Republic of Korea

H. Ahn
Industrial Technology Convergence Center
Pohang Accelerator Laboratory
Pohang University of Science and Technology (POSTECH)
Pohang 37673, Republic of Korea

Table of Contents

Experimental Section

Materials

Diethylene glycol monomethyl ether, triethylene glycol monomethyl ether, tetra ethylene glycol monomethyl ether, penta ethylene glycol monomethyl ether, 1,6-dibromohexane, sodium hydride (60% dispersion in mineral oil), *N*-bromosuccinimide and tetrakis(triphenylphosphine)palladium(0) ($Pd(PPh_3)_4$) and were purchased from Sigma-Aldrich. Potassium carbonate was purchased from Samchun Chemicals. 3,6-Di(thiophen-2-yl)pyrrolo[3,4-*c*]pyrrole-1,4(2*H*,5*H*)-dione and 2,2'-bithiophene-5,5'-bis(trimethylstannane) were purchased from Derthon Optoelectronic Materials Science Technology Co LTD. All the materials were used without further purification.

Characterizations

Chemical structural analysis. ^{1}H and ^{13}C nuclear magnetic resonance (NMR) spectra were recorded using a Bruker Avance 400 MHz spectrometer. Chloroform-*d* solutions of monomers and their precursors were prepared at the concentration of 2 mg mL^{-1} and 40 mg mL^{-1} for ^{1}H and ^{13}C NMR measurements, respectively. 1,1,2,2-Tetrachloroethane-d_2 solutions of polymers (10 mg mL^{-1}) were used for the ^{1}H NMR measurement.

Mass analysis. For matrix-assisted laser desorption ionization-time of flight mass spectrometry (MALDI-ToF MS), molecular weight distributions of the polymers were investigated using a positive linear mode of Bruker autoflex Ⅲ and *trans*-2-[3-(4-*tert*-butylphenyl)-2-methyl-2-propenylidene]malononitrile as a matrix.

Optical analysis. To obtain UV–Vis absorption spectra, the polymer solutions in chloroform at the concentration of 0.02 mg mL^{-1} and chloroform-processed polymer films were used. For

polarized UV–Vis absorption spectra, a linear polarizing film was applied depending on the orientation. A dichroic ratio (DR) was calculated as the ratio of absorbance (A_1 / A_2, where A is a peak absorbance) depending on the polarizing angle. The corresponding 2D order parameter ($S_{2.mol}$) is calculated as (DR − 1)/(DR + 1).

Spectroelectrochemical analysis. Measurement was performed using Cary 5000 UV−Vis−NIR spectrophotometer. Change in absorption spectra was recorded for chloroform-processed polymer films on indium tin oxide (ITO)/glass substrates immersed in 0.1 M NaCl aqueous solution, depending on the potential applied to the films. The potential *versus* Ag/AgCl reference electrode was changed from 0 V to 0.8 V with an interval of 0.1 V.

Electrochemical analysis. Cyclic voltammograms (CV) were obtained using a common three-electrode system with a VSP Potentiostat from BioLogic and EC-Lab software. Measurement was performed in both NaCl (0.1 M in water) and tetrabutylammonium hexafluorophosphate (0.1 M in acetonitrile) electrolyte with the scan rate was 50 mV s^{-1}. The electrolyte was degassed with argon for 10 min before each measurement.

Electrochemical Impedance Spectroscopy (EIS) analysis. Characterization was performed with an electrochemical workstation (Metrohm-Autolab, PGSTAT 302N), using a 0.1 M NaCl aqueous solution with an Ag/AgCl reference electrode and a Pt sheet-type counter electrode, at the frequency range between 0.1 to 100 kHz with sinusoidal signals of E_{ac} = 25 mV at E_{dc} = 0 V. For sample preparation, active layers were coated on Au-coated glass substrates as the working electrode, while the rest of the exposed area of the active layer was passivated using epoxy glue. The aqueous electrolyte solution (0.1 M NaCl) degassed by nitrogen gas for 30 min was employed for all EIS measurements. The acquired curve was fitted with [R_s (R_p·C_p)]

model using Nova software (Metrohm-Autolab). Next, the fitted C_p value was normalized with the corresponding polymer film volume as shown in the following equation:

$$C^* = \frac{C_P}{d \cdot A}$$

where C^*, d, A are volumetric capacitance, film thickness, and exposed active layer area, respectively.

Fabrication and characterization of OECTs: For the fabrication of OECTs on glass substrates, gold (Au, 45 nm) and chrome (Cr, 5 nm) were utilized as the source and drain electrodes, which were patterned by photolithography. Prior to the deposition of the patterned electrodes on the substrates, they were cleaned under ultrasonication using acetone (10 min) and isopropanol (10 min) and subsequently dried by blowing nitrogen. Active materials were dissolved in chloroform to the concentration of 10 mg mL^{-1}. To prepare the OECT active films, the polymer solutions were spin-coated on the substrates at 2500 rpm for 60 s. It is noted that any pre- or post-treatment was not applied to improve the morphology of polymer films. For active layer patterning, CYTOP (CTL-809M, Asahi Glass Co.) was spin-coated at 2000 rpm and then baked at 100 °C for 1 h. For the hydrophilicity of the CYTOP surface, O_2 plasma was treated for 5 s, and positive photoresist (GXR-601, Microchemicals GmbH) was spin-coated and patterned through conventional photolithography. After immersion in fluorosolvent (NOVEC 7200, 3M) to dissolve CYTOP, stirred at 50 °C, overnight. The fabricated OECT active layer had a channel length of 20 μm and a channel width of 80 μm. The performance parameters of the OECTs were measured using a Keithley 2400 source meter and customized MATLAB code, while an Ag/AgCl electrode and an aqueous solution

(0.1 M NaCl) were employed as the gate electrode and the electrolyte of OECTs, respectively. Note that the aqueous electrolyte solution (0.1 M NaCl) was degassed by bubbling nitrogen gas for 30 min and all OECT characterizations were performed in a nitrogen-purged glove box. Film thickness values used for OECT characterizations and C^* calculation were measured using a Dektak profilometer.

Fabrication and characterization of OFETs: OFET devices were fabricated as bottom-gate top-contact device architecture. A highly doped Si wafer was used as a gate electrode, and 200 nm-thick SiO_2 with a specific capacitance (C_i) of 17.3 nF cm^{-2} was used as a gate dielectric. Octadecyltrichlorosilane (ODTS) was treated with SiO_2 and polymer solutions of a concentration of 10 mg mL^{-1} in chloroform were spin-casted onto ODTS-treated SiO_2/Si substrates at 2500 rpm for 60 s. Then, 70 nm-thick Au was deposited by thermal evaporation using a patterned shadow mask. The electrical properties of OFET devices were measured with a Keithley 4200. The metal-oxide semiconductor field-effect transistor (MOSFET) equation used for the calculation of the parameters is

$$I_D = \frac{1}{2}\frac{W}{L}\mu C_i(V_G - V_{th})^2$$

where I_D is the drain current, V_G is the gate voltage, V_{th} is the threshold voltage, and C_i is the specific capacitance of the dielectric layer.

Thermal admittance spectroscopy (TAS) analysis: The devices were prepared with the architecture of ITO/PEDOT:PSS/polymer/PNDIT-F3N-Br/Ag. The frequency-dependent capacitance response was obtained using an impedance analyzer (IVIUM tech., CompactStat) ranging from 1 Hz to 1 MHz at zero bias with a modulated signal of 20 mV under dark

condition. The frequency-capacitance response was converted to the trap density of states (tDOS) distribution corresponding to the trap level using the following equation:

$$N_T(E_\omega) = -\frac{V_{bi}}{qW}\frac{dC}{d\omega}\frac{\omega}{k_B T}$$

where W is the width of a dielectric layer, C is the capacitance, ω is the angular frequency, q is the electric charge, k_B is the Boltzmann's constant, T is the temperature, and V_{bi} is the built-in potential defined as the internal electric field between electrodes under short-circuit condition. [1, 2] In this study, we set the V_{bi} value of 0.77 V based on the work function difference between the anode (ITO, −4.70 eV) and cathode (Ag/PNDIT-F3N-Br, −3.93 eV). The trap level (E_ω) with corresponding to an applied angular frequency ω_0 is given by:[3]

$$E_\omega = k_B T \ln\left(\frac{\omega_0}{\omega}\right)$$

where ω_0 is attempt-to-escape frequency.

Microstructural analysis. For grazing-incidence X-ray scattering (GIXS) measurements, as-cast polymer films were prepared by spin-casting polymers in chloroform solutions on ITO substrates, each with a 1 cm × 1 cm square shape. To prepare the oxidized samples, the films were oxidized in a 0.1 M NaCl aqueous electrolyte by adjusting the potential *versus* Ag/AgCl reference to 0.8V. GIXS analyses were performed at the 9A beamline in Pohang Accelerator Laboratory, Republic of Korea. Beam damage was minimized by measuring samples for a short exposure time of less than 10 s in a vacuum (~ 10^{-3} torr). Also, to prevent beam damage during sample alignment, an X-ray attenuator was used for the beam intensity to be reduced tenfold. The sample-to-detector distance was 222.429 mm. The incidence angle of X-ray was 0.12° to penetrate the full height of thin films and the beam energy was 11.08 keV. The incident beam had an ellipsoid shape with horizontal and vertical dimensions of 320 μm and 60 μm, respectively. The detector (MX170-HS from Rayonix) was used, which had a

detection dimension of 170 mm × 170 mm, a pixel number of 1920 × 1920, and a pixel size of 0.089 mm. The beam calibration was proceeded by using a pre-calibrated reference, sucrose, and calibrating a pixel diffraction angle. Corrected (missing wedge-shaped) 2D GIXS images and the corresponding line-cut profiles were extracted using customized MATLAB scripts. The crystal coherence lengths (L_cs) of reflection peaks were calculated from the following Scherrer equation,

$$L_c = \frac{2\pi K}{\Delta q}$$

where K and Δq are the shape factor (the value of 0.9 was applied in this work) and the full width at half maximum (FWHM) of diffraction peaks, respectively. To calculate FWHMs of (100) and (010) scattering peaks, a Gaussian fitting for each peak was carried out. The paracrystalline disorder parameter (g) values were estimated from the following equation,

$$g \approx \frac{1}{2\pi}\sqrt{\Delta q \cdot d}$$

where d is the interplanar spacing of diffraction peaks.

Thermal analysis. For differential scanning calorimetry (DSC) sample preparation, bulk polymer samples were collected in DSC pans. Thermal properties were extracted from the first heating cycles from 20 to 285 °C at a rate of 2 °C min^{-1} by a TA Instruments DSC 25.

Unidirectional Floating Film Transfer Method (UFTM). The active material (PDPP-4EG) was dissolved in chloroform to the concentration of 10 mg mL^{-1}. The liquid substrate for polymer transfer was prepared by combining ethylene glycol and glycerol in a volumetric ratio of 3:1. The mixture was then poured into a glass bath positioned on a hot plate preheated to 55 °C. A custom-made slide was carefully placed in the bath. Subsequently, 15 μL of polymer solution was dispensed onto the interface between the glass slide and the liquid substrate. The

elongated polymer film was transferred onto a pre-cleaned substrate, rinsed with ethanol to eliminate any residue, and dried using nitrogen gas. To obtain sufficiently thick active channels (~60 nm), the polymer films were stacked through three times of film transfer. It was confirmed through AFM measurement that there was no significant deviation in thickness depending on the position of polymer films. The rest of device fabrication and characterization procedures were same as those of conventional OECTs based on spin-cast polymer films.

Synthesis

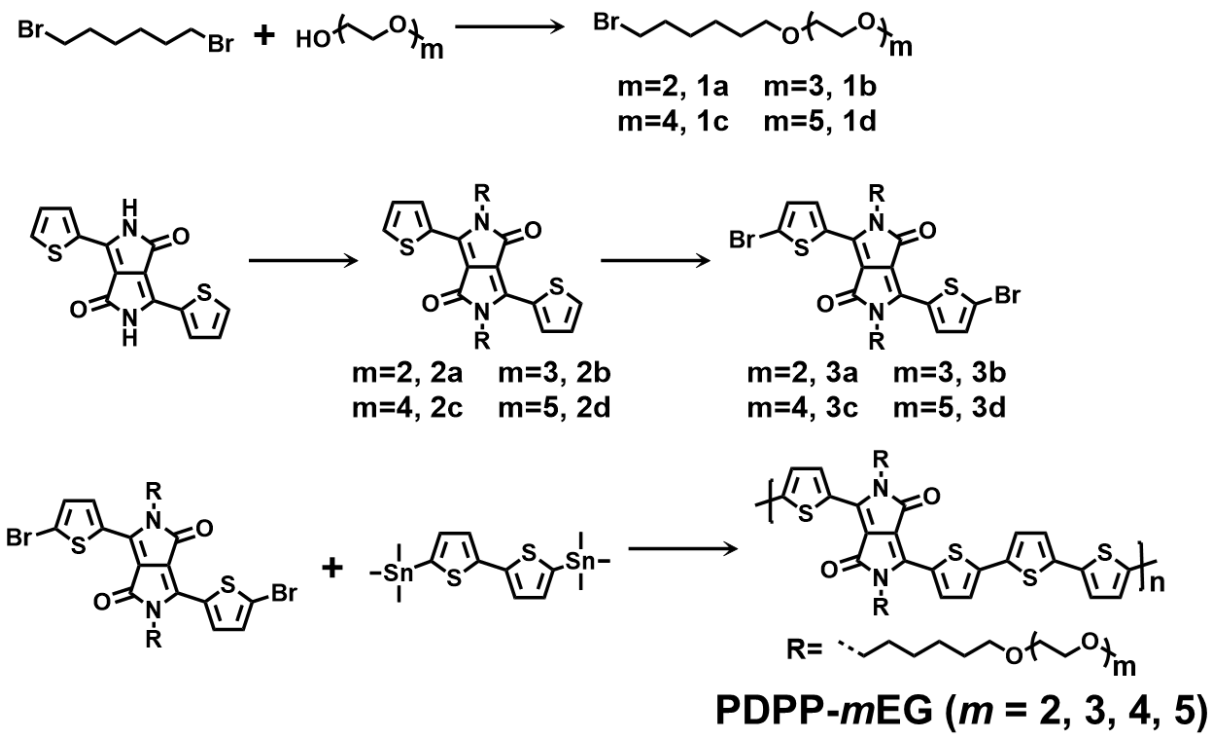

Scheme S1. Synthetic routes to monomers and polymers.

Compound 1a: Diethylene glycol monomethyl ether (11.0 g, 92 mmol) was added dropwise using a syringe to a mixture of NaH (60% dispersion in mineral oil, 5.5 g, 137 mmol) and 1,6-dibromohexane (67.0 g, 275 mmol) in THF (50 mL) in a one-necked flask. The resulting mixture was stirred at room temperature overnight. Then, the mixture was quenched with water. The organic phase was washed with deionized water, extracted with chloroform, dried with anhydrous magnesium sulfate ($MgSO_4$), and filtered. The residual solvent was removed by rotary evaporation. The crude product was purified using column chromatography on silica gel with a dichloromethane (DCM)/acetone solvent mixture (9:1 v/v) as an eluent to yield a colorless liquid (19.7 g, 76%). ^{1}H NMR (400 MHz, chloroform-*d*) δ 3.66–3.62 (m, 4H), 3.61–3.53 (m, 4H), 3.46 (t, *J* = 6.6 Hz, 2H), 3.40 (t, *J* = 6.8 Hz, 2H), 1.90–1.81 (m, 2H), 1.63–1.55 (m, 2H), 1.49–1.41 (m, 2H), 1.41–1.32 (m, 2H).

Compound 1b: Diethylene glycol monomethyl ether for the synthesis of compound 1a was replaced with triethylene glycol monomethyl ether using the same molar stoichiometry. The rest of synthetic procedure was same as that of compound 1a (22.2 g, 74% yield). ^{1}H NMR

(400 MHz, chloroform-*d*) δ 3.68 – 3.62 (m, 8H), 3.59–3.53 (m, 4H), 3.45 (t, *J* = 6.6 Hz, 2H), 3.40 (t, *J* = 6.8 Hz, 2H), 1.90–1.82 (m, 2H), 1.63–1.55 (m, 2H), 1.49–1.40 (m, 2H), 1.40–1.33 (m, 2H).

Compound 1c: Diethylene glycol monomethyl ether for the synthesis of compound 1a was replaced with tetraethylene glycol monomethyl ether using the same molar stoichiometry. The rest of synthetic procedure was same as that of compound 1a (23.1 g, 68% yield). ^{1}H NMR (400 MHz, chloroform-*d*) δ 3.68–3.62 (m, 12H), 3.59–3.53 (m, 4H), 3.45 (t, *J* = 6.7 Hz, 2H), 3.40 (t, *J* = 6.8 Hz, 2H), 1.90–1.81 (m, 2H), 1.63–1.54 (m, 2H), 1.49 – 1.41 (m, 2H), 1.41 – 1.32 (m, 2H).

Compound 1d: Diethylene glycol monomethyl ether for the synthesis of compound 1a was replaced with pentaethylene glycol monomethyl ether using the same molar stoichiometry. The rest of synthetic procedure was same as that of compound 1a (26.2 g, 69% yield). ^{1}H NMR (400 MHz, chloroform-*d*) δ 3.68–3.61 (m, 16H), 3.59–3.53 (m, 4H), 3.45 (t, *J* = 6.6 Hz, 2H), 3.40 (t, *J* = 6.8 Hz, 2H), 1.90–1.81 (m, 2H), 1.64–1.55 (m, 2H), 1.50–1.41 (m, 2H), 1.41–1.32 (m, 2H).

Compound 2a: To a solution of 3,6-di(thiophen-2-yl)pyrrolo[3,4-*c*]pyrrole-1,4(2*H*,5*H*)-dione (3.0 g, 10 mmol) in *N*,*N*-dimethylformamide (60 mL) in a nitrogen-purged one-necked flask, potassium carbonate (5.5 g, 40 mmol) was added. The mixture was stirred at 140 ºC for 1 h. Then, compound 1a (8.5 g, 30 mmol) was added slowly and the mixture was further stirred at 140 ºC overnight. After cooling the mixture, the organic phase was washed with deionized water, extracted with chloroform, dried with anhydrous $MgSO_4$, and filtered. The residual solvent was removed by rotary evaporation. The crude product was purified using column chromatography on silica gel with a DCM/acetone solvent mixture (7:3 v/v) as an eluent to yield a purple solid (4.9 g, 70%). ^{1}H NMR (400 MHz, chloroform-*d*) δ 8.92 (dd, *J* = 3.9, 1.2 Hz, 2H), 7.64 (dd, *J* = 5.0, 1.2 Hz, 2H), 7.29 (dd, *J* = 5.0, 3.9 Hz, 2H), 4.07 (t, *J* = 6.7 Hz, 4H), 3.66–3.62 (m, 8H), 3.60–3.53 (m, 8H), 3.44 (t, *J* = 6.6 Hz, 4H), 1.80–1.70 (m, 4H), 1.63–1.54 (m, 4H), 1.49–1.35 (m, 8H).

Compound 2b: Compound 1a for the synthesis of compound 2a was replaced with compound 1b using the same molar stoichiometry. The rest of synthetic procedure was same as that of

compound 2a (5.9 g, 67% yield). ^{1}H NMR (400 MHz, chloroform-*d*) δ 8.92 (dd, *J* = 3.9, 1.2 Hz, 2H), 7.64 (dd, *J* = 5.0, 1.2 Hz, 2H), 7.28 (dd, *J* = 5.1, 3.9 Hz, 2H), 4.07 (t, *J* = 6.7 Hz, 4H), 3.67–3.61 (m, 16H), 3.59 – 3.52 (m, 8H), 3.44 (t, *J* = 6.7 Hz, 4H), 1.80–1.70 (m, 4H), 1.63–1.54 (m, 4H), 1.48–1.35 (m, 8H).

Compound 2c: Compound 1a for the synthesis of compound 2a was replaced with compound 1c using the same molar stoichiometry. The rest of synthetic procedure was same as that of compound 2a (5.9 g, 66% yield). ^{1}H NMR (400 MHz, chloroform-*d*) δ 8.92 (dd, *J* = 3.8, 1.2 Hz, 2H), 7.64 (dd, *J* = 5.0, 1.2 Hz, 2H), 7.29 (dd, *J* = 4.4, 3.9 Hz, 2H), 4.07 (t, *J* = 7.9 Hz, 4H), 3.68–3.60 (m, 24H), 3.60–3.52 (m, 8H), 3.44 (t, *J* = 6.8 Hz, 4H), 1.81–1.70 (m, 4H), 1.65–1.54 (m, 4H), 1.48–1.34 (m, 8H).

Compound 2d: Compound 1a for the synthesis of compound 2a was replaced with compound 1d using the same molar stoichiometry. The rest of synthetic procedure was same as that of compound 2a (5.6 g, 58% yield). ^{1}H NMR (400 MHz, chloroform-*d*) δ 8.92 (dd, *J* = 3.8, 1.2 Hz, 2H), 7.64 (dd, *J* = 5.0, 1.2 Hz, 2H), 7.29 (dd, *J* = 4.4, 3.9 Hz, 2H), 4.07 (t, *J* = 7.9 Hz, 4H), 3.68–3.60 (m, 32H), 3.60–3.52 (m, 8H), 3.44 (t, *J* = 6.8 Hz, 4H), 1.80–1.70 (m, 4H), 1.65–1.54 (m, 4H), 1.48–1.35 (m, 8H).

Compound 3a: Compound 2a (4.9 g, 7.0 mmol) in chloroform was prepared in a flask and under dark condition. NBS (2.5 g, 14.6 mmol) was added in several portions and the resulting mixture was stirred at room temperature overnight. The organic phase was washed with deionized water, extracted with chloroform, dried with anhydrous $MgSO_4$, and filtered. The residual solvent was removed by rotary evaporation. The crude product was purified using column chromatography on silica gel with a DCM/acetone solvent mixture (8:2) as an eluent and recrystallized using methanol/chloroform solvent mixture to yield a purple solid (4.7 g, 78%). ^{1}H NMR (400 MHz, chloroform-*d*) δ 8.67 (d, *J* = 4.2 Hz, 2H), 7.24 (d, *J* = 4.2 Hz, 2H), 3.98 (t, *J* = 7.8 Hz, 4H), 3.66–3.62 (m, 8H), 3.60–3.53 (m, 8H), 3.45 (t, *J* = 6.6 Hz, 4H), 1.77–1.67 (m, 4H), 1.64–1.55 (m, 4H), 1.48–1.36 (m, 8H). ^{13}C NMR (101 MHz, $CDCl_3$) δ 161.25, 139.18, 135.59, 131.90, 131.27, 119.40, 108.01, 77.55, 77.23, 76.91, 72.17, 71.47, 70.87, 70.76, 70.31, 59.27, 42.38, 31.15, 30.20, 29.71, 26.91, 25.98.

Compound 3b: Compound 2a was replaced with compound 2b using the same molar

stoichiometry. The rest of synthetic procedure was same as that of compound 3a (5.7 g, 80% yield). ^{1}H NMR (400 MHz, chloroform-*d*) δ 8.67 (d, *J* = 4.2 Hz, 2H), 7.24 (d, *J* = 4.2 Hz, 2H), 3.98 (t, *J* = 7.8 Hz, 4H), 3.68–3.61 (m, 16H), 3.59–3.52 (m, 8H), 3.45 (t, *J* = 6.6 Hz, 4H), 1.77–1.67 (m, 4H), 1.64–1.54 (m, 4H), 1.48–1.36 (m, 8H). ^{13}C NMR (101 MHz, $CDCl_3$) δ 161.25, 139.19, 135.60, 131.91, 131.27, 119.40, 108.01, 77.55, 77.23, 76.91, 72.16, 71.47, 70.84, 70.81, 70.74, 70.31, 59.26, 42.39, 30.20, 29.72, 26.92, 25.98.

Compound 3c: Compound 2a was replaced with compound 2c using the same molar stoichiometry. The rest of synthetic procedure was same as that of compound 3a (5.1 g, 73% yield). ^{1}H NMR (400 MHz, chloroform-*d*) δ 8.67 (d, *J* = 4.2 Hz, 2H), 7.24 (d, *J* = 4.2 Hz, 2H), 3.98 (t, *J* = 7.8 Hz, 4H), 3.68–3.61 (m, 24H), 3.59–3.52 (m, 8H), 3.44 (t, *J* = 6.6 Hz, 4H), 1.77–1.67 (m, 4H), 1.64–1.55 (m, 4H), 1.48–1.36 (m, 8H). ^{13}C NMR (101 MHz, $CDCl_3$) δ 161.24, 139.19, 135.60, 131.91, 131.27, 119.41, 108.01, 77.55, 77.23, 76.91, 72.15, 71.48, 70.82, 70.79, 70.73, 70.32, 59.26, 42.39, 30.20, 29.72, 26.92, 25.98.

Compound 3d: Compound 2a was replaced with compound 2d using the same molar stoichiometry. The rest of synthetic procedure was same as that of compound 3a (4.8 g, 73% yield). ^{1}H NMR (400 MHz, chloroform-*d*) δ 8.67 (d, *J* = 4.2 Hz, 2H), 7.24 (d, *J* = 4.2 Hz, 2H), 3.98 (t, *J* = 7.8 Hz, 4H), 3.69–3.60 (m, 32H), 3.59–3.52 (m, 8H), 3.44 (t, *J* = 6.6 Hz, 4H), 1.78–1.69 (m, 4H), 1.64–1.55 (m, 4H), 1.48–1.35 (m, 8H). ^{13}C NMR (101 MHz, $CDCl_3$) δ 161.23, 139.18, 135.59, 131.90, 131.26, 119.40, 108.00, 77.55, 77.23, 76.91, 72.15, 71.47, 70.82, 70.80, 70.79, 70.73, 70.31, 59.26, 42.38, 30.19, 29.71, 26.92, 25.97.

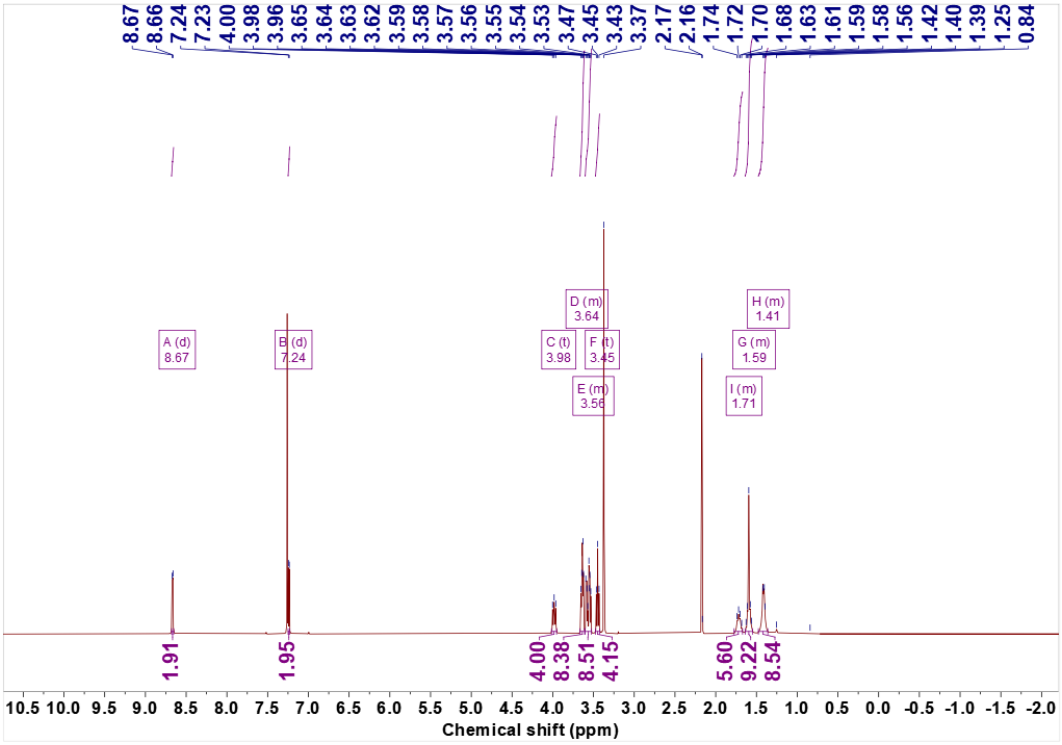

Figure S1. ^{1}H NMR spectrum of Compound 3a.

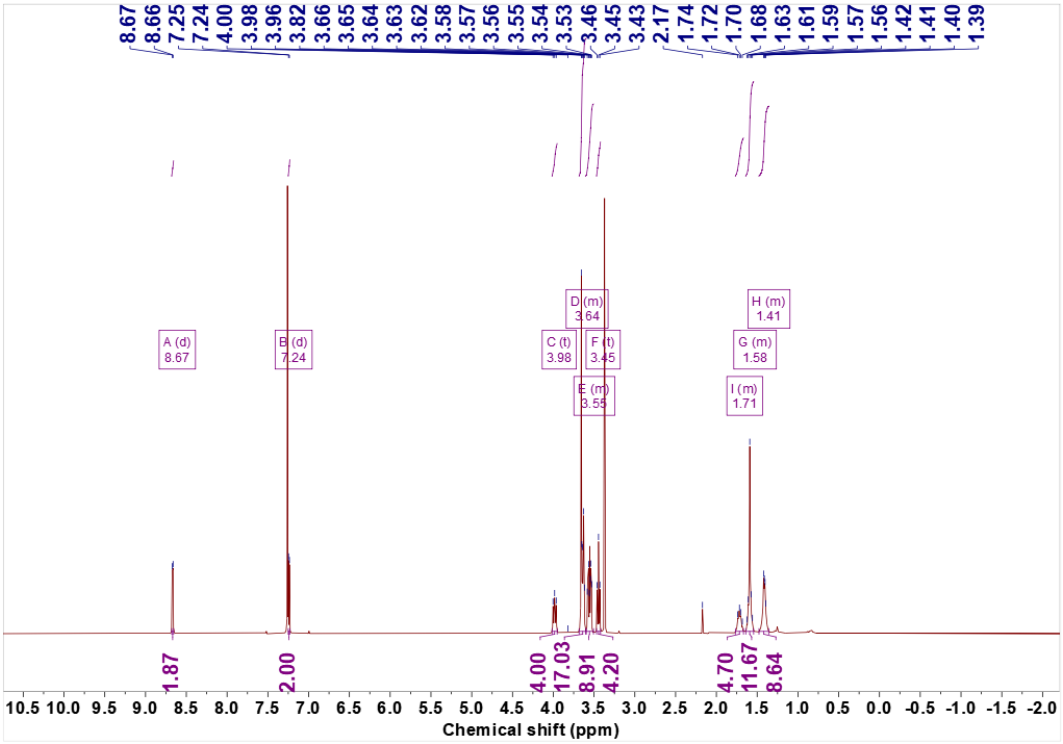

Figure S2. ^{1}H NMR spectrum of Compound 3b.

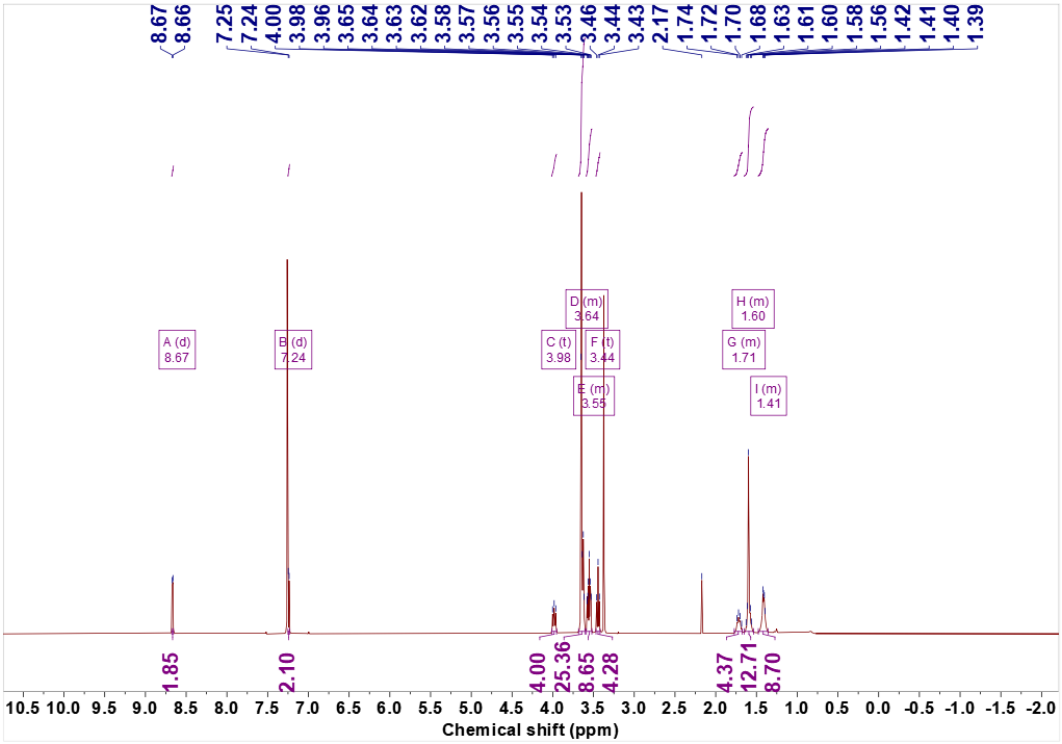

Figure S3. ^{1}H NMR spectrum of Compound 3c.

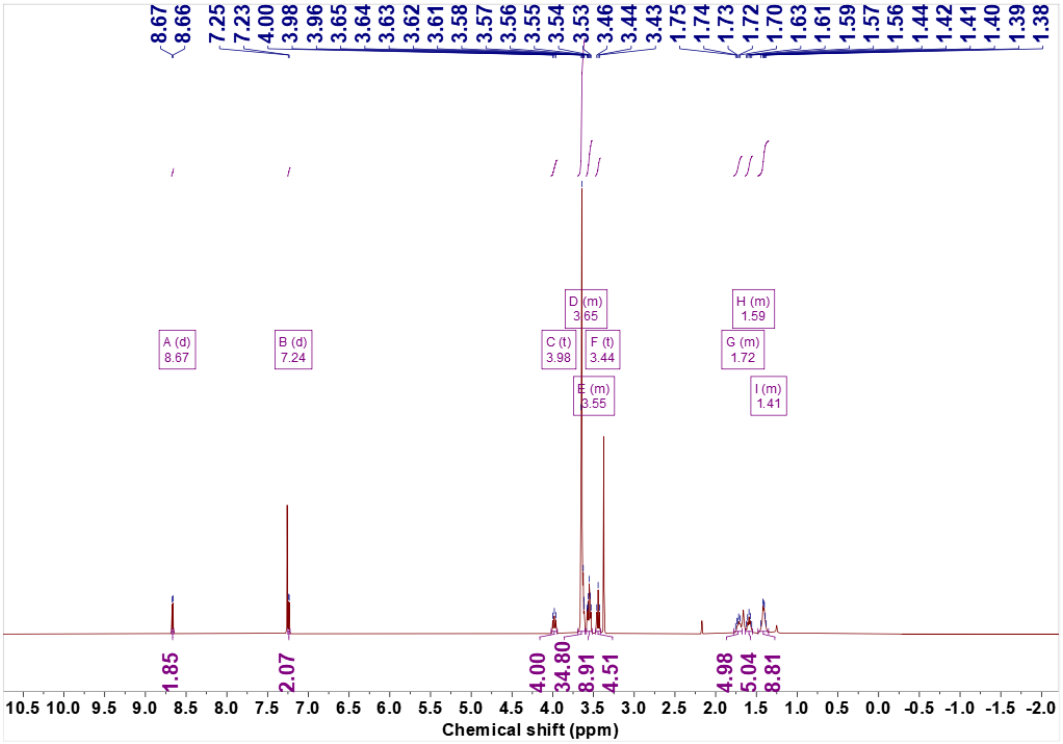

Figure S4. ^{1}H NMR spectrum of Compound 3d.

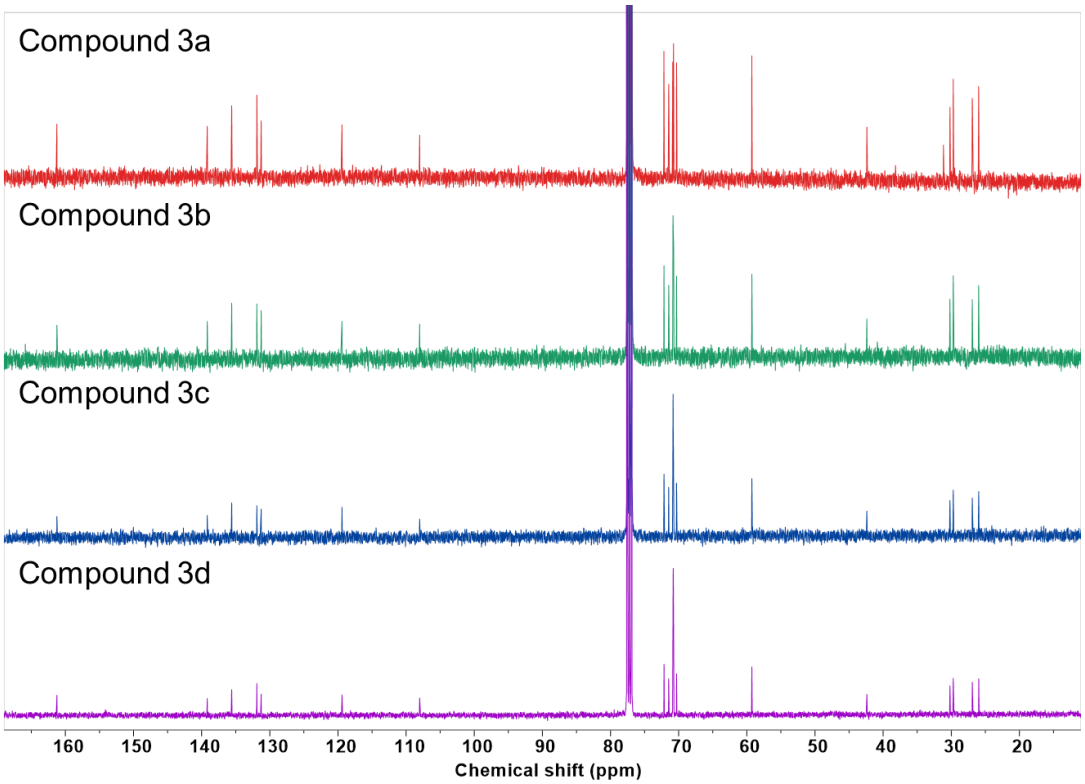

Figure S5. ^{13}C NMR spectra of the monomers.

PDPP-2EG: In a 20 mL vial, compound 3a (86.7 mg, 0.1 mmol), 2,2'-bithiophene-5,5'-bis(trimethylstannane) (49.2 mg, 0.1 mmol), $Pd(PPh_3)_4$ catalyst (3.1 mg, 3 μmol) were dissolved in 2.5 mL chlorobenzene. After purging with argon, the solution was stirred at the temperature of 120 ºC for 4 h. The crude product was precipitated in methanol and purified through Soxhlet extraction. The polymer was sequentially washed with methanol, acetone, and hexane and extracted from chloroform. The chloroform fraction was roughly dried using a rotary evaporator and fully dried in a high vacuum (58 mg, 67% yield). ^{1}H NMR (400 MHz, 1,1,2,2-tetrachloroethane-d_2) δ 8.92 – 8.86 (m), 8.59 – 8.55 (m), 7.39–7.05 (m), 4.17–4.07 (m), 4.06–4.00 (m), 3.68–3.47 (m), 3.39 (d, J = 5.2 Hz), 1.88–1.75 (m), 1.71–1.60 (m), 1.58–1.43 (m), 1.39–1.28 (m).

PDPP-3EG: The synthetic procedure was same as that of PDPP-2EG (75 mg, 78% yield). ^{1}H NMR (400 MHz, 1,1,2,2-tetrachloroethane-d_2) δ 8.85 (br s), 6.83 (br s), 4.00–3.30 (m), 2.00–1.16 (m).

PDPP-4EG: The synthetic procedure was same as that of PDPP-2EG (74 mg, 71% yield). ^{1}H

NMR (400 MHz, 1,1,2,2-tetrachloroethane-d_2) δ 8.83 (br s), 6.79 (br s), 4.04–3.29 (m), 2.10–1.20 (m).

PDPP-5EG: The synthetic procedure was same with that of PDPP-2EG (70 mg, 62% yield). ^{1}H NMR (400 MHz, 1,1,2,2-tetrachloroethane-d_2) δ 8.89 (br s), 6.92 (br s), 3.90–3.33 (m), 2.20–1.23 (m).

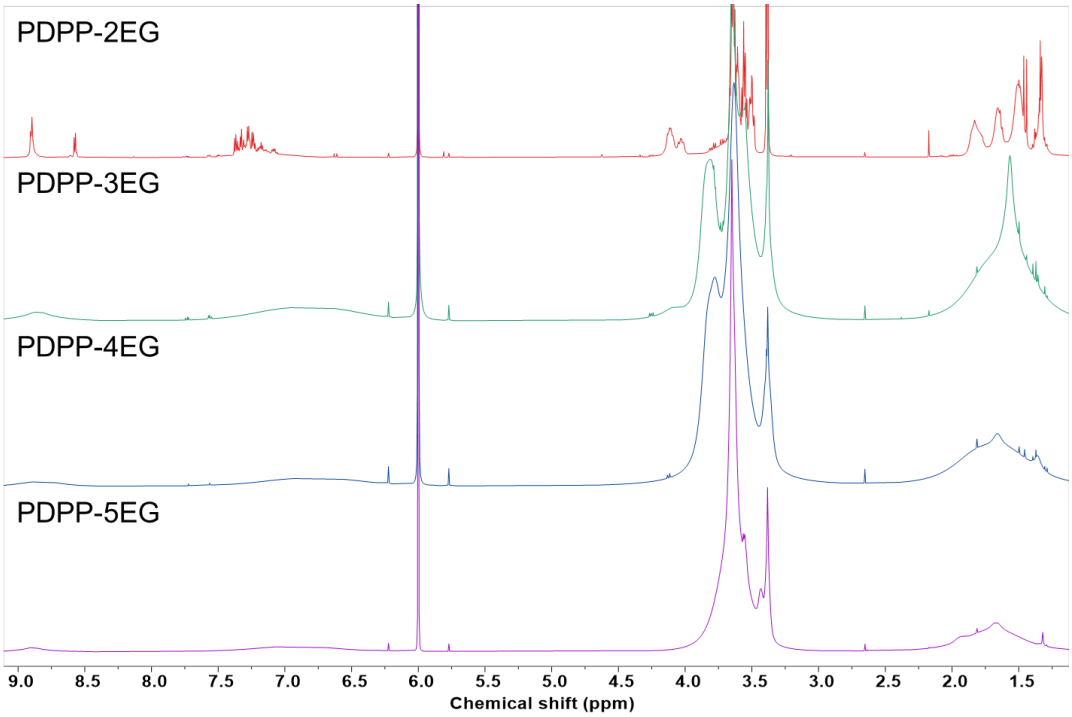

Figure S6. ^{1}H NMR spectra of the polymers.

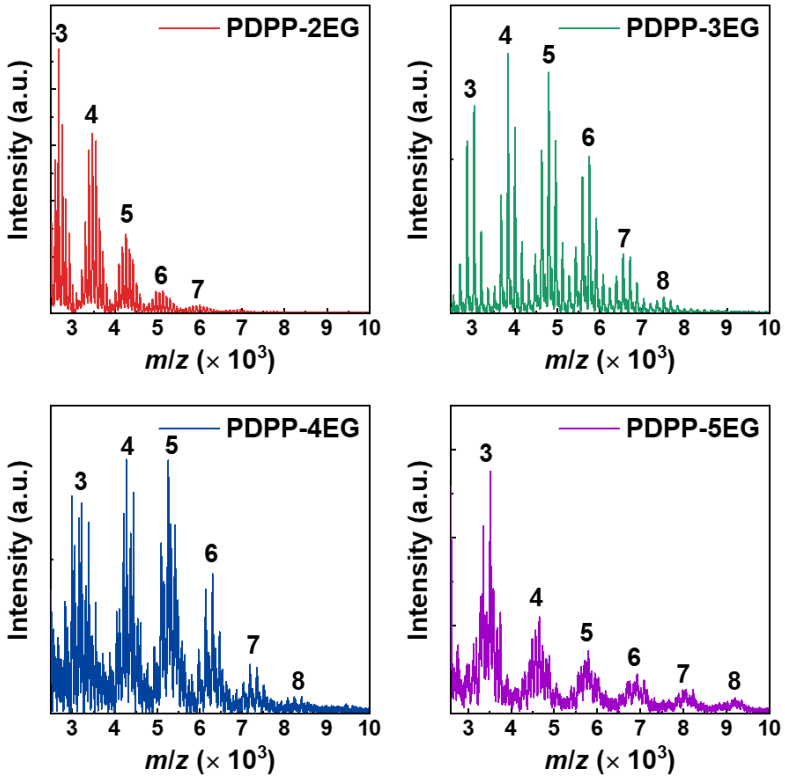

Figure S7. MALDI-ToF mass spectra of the polymers. The number of DPP units corresponding to each molecular weight is notated above each peak.

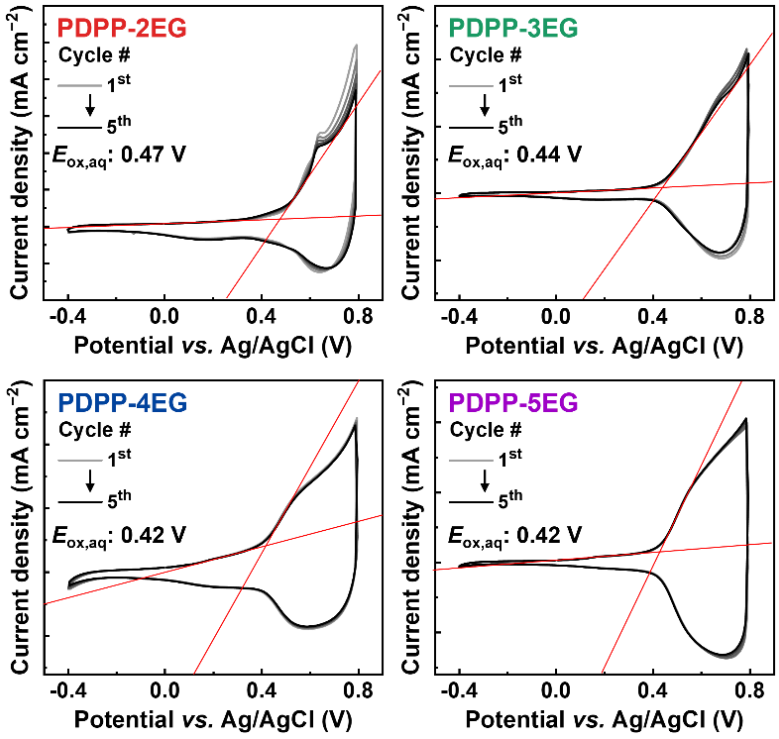

Figure S8. Electrochemical stability tests of PDPP-*m*EG polymers by running 5 charging/discharging cycles in a 0.1 M NaCl aqueous electrolyte. The red-colored tangents were used to determine the oxidation onsets.

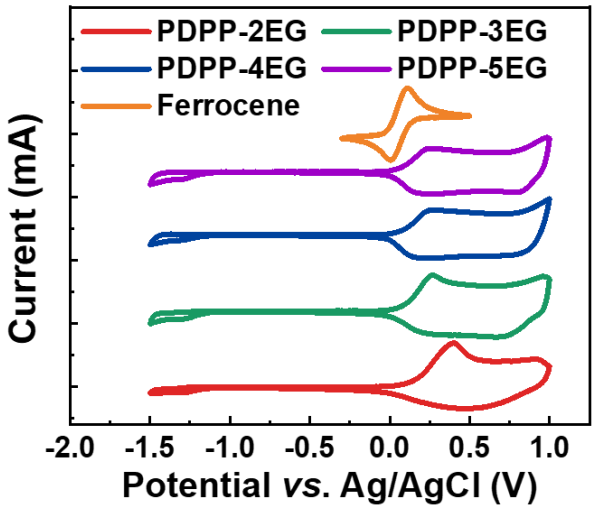

Figure S9. Cyclic voltammograms of the polymer films in 0.1 M tetrabutylammonium hexafluorophosphate in *N*,*N*-dimethylformamide as an organic electrolyte.

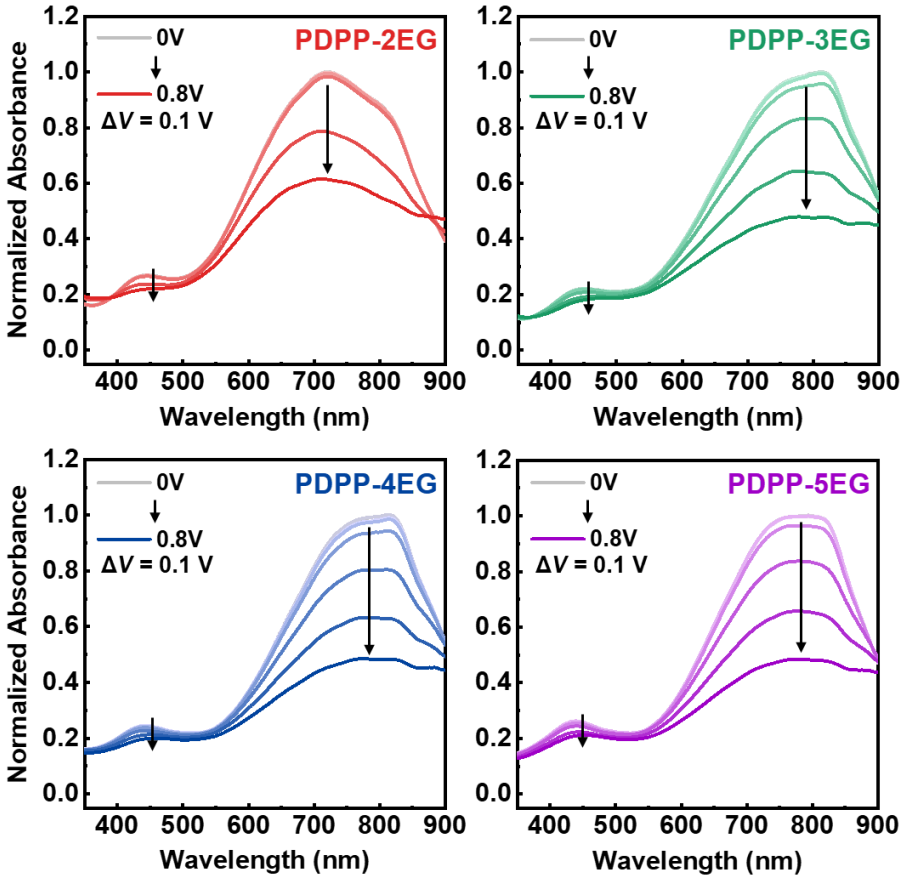

Figure S10. Spectroelectrochemical UV–Vis absorption spectra of the polymer films in a 0.1 M NaCl aqueous electrolyte.

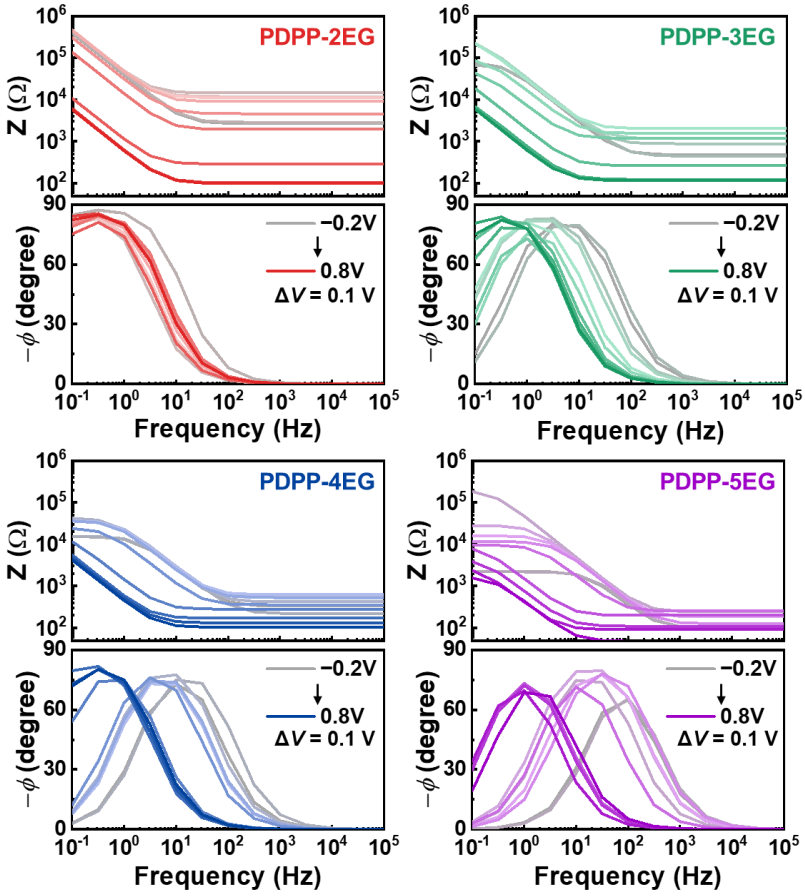

Figure S11. EIS curves for the polymers at different offset DC voltages relative to the Ag/AgCl electrode.

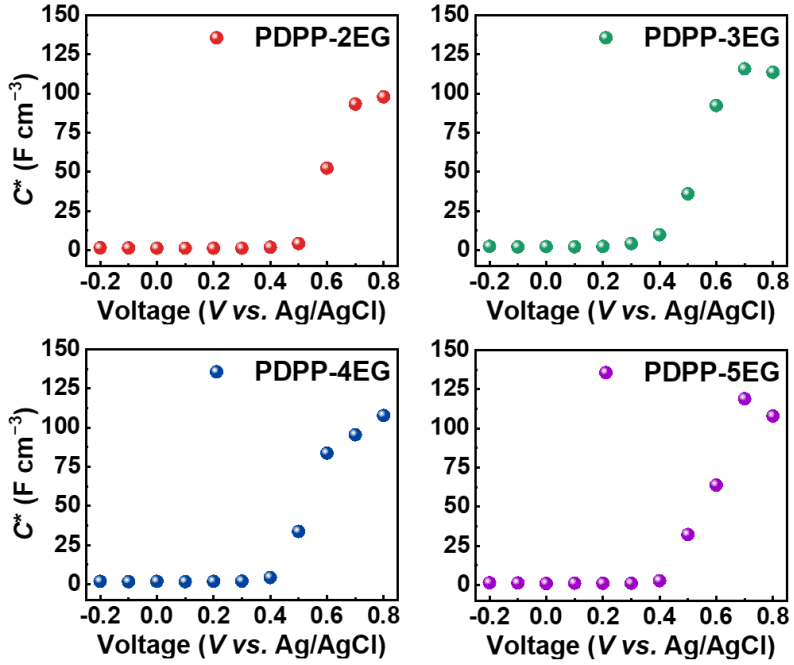

Figure S12. Volumetric capacitances of the polymers depending on the voltage of the working electrode calculated from EIS measurement.

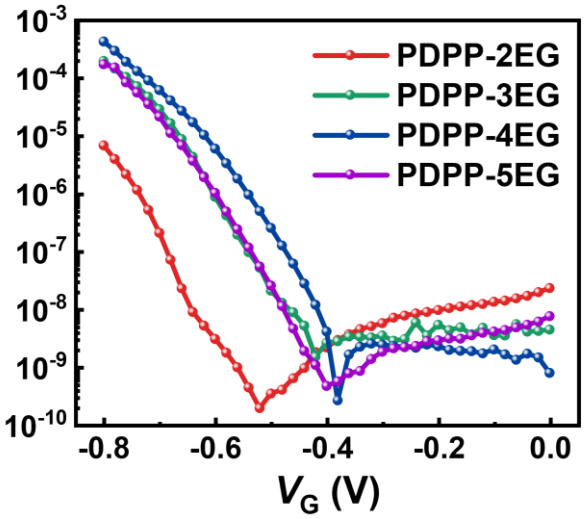

Figure S13. Representative log-scale transfer curves of PDPP-*m*EG-based OECTs.

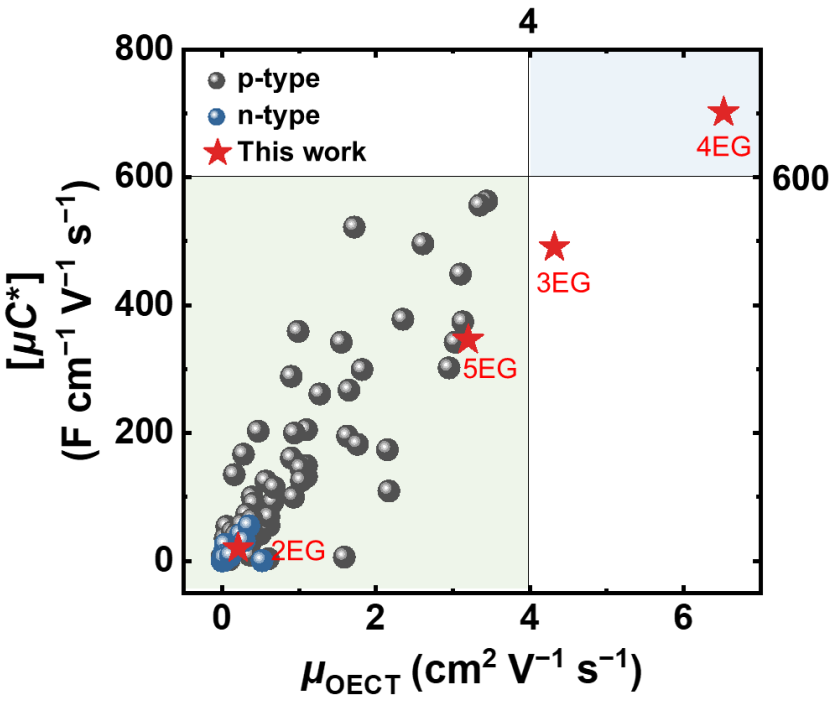

Figure S14. μ_{OECT}–[μC^*] plots for accumulation-mode OECTs. For a fair comparison, only OECT devices using NaCl, KCl, or phosphate buffered saline (PBS) solutions as gate electrolytes were considered.

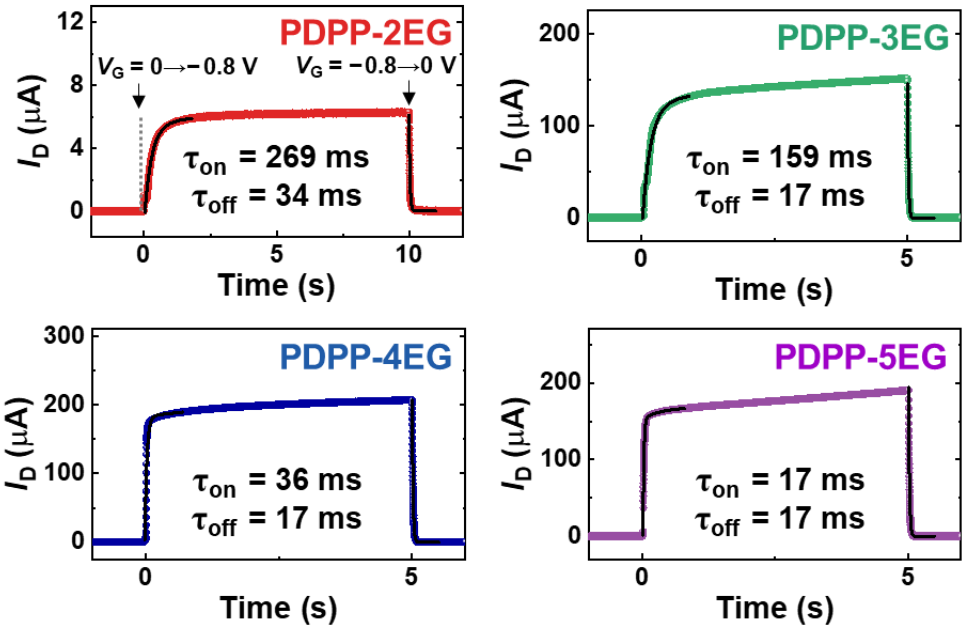

Figure S15. Transient characteristics of OECTs.

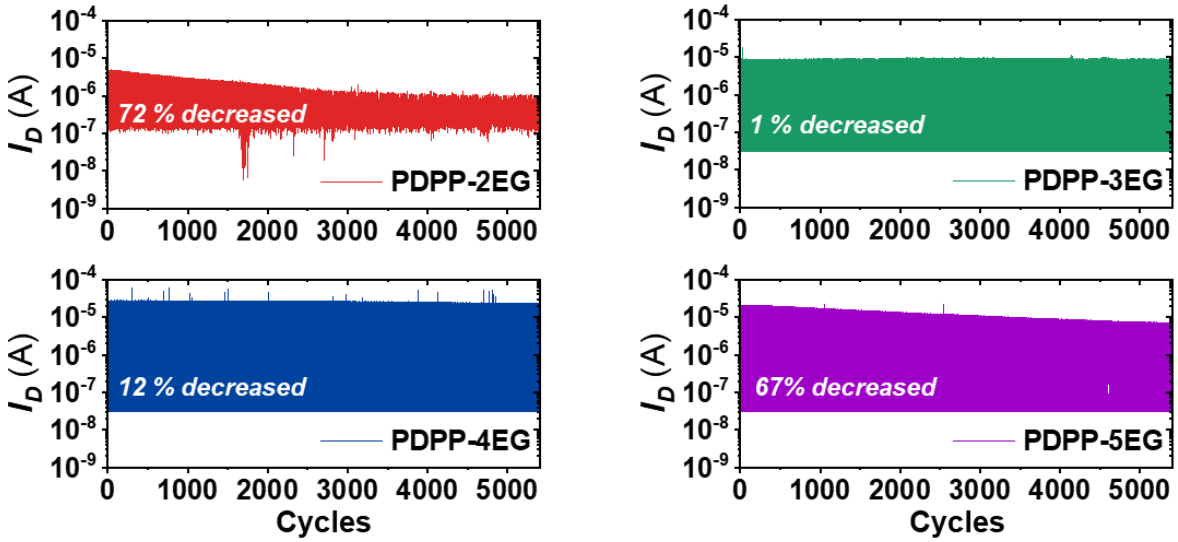

Figure S16. Operational stability of OECT devices. The stability tests were conducted by switching on (V_G = −0.7 V) and off (V_G = 0 V) every 4.5 s and the active channels were subjected to the continuous doping and dedoping cycles by 600 times for 1.5 h.

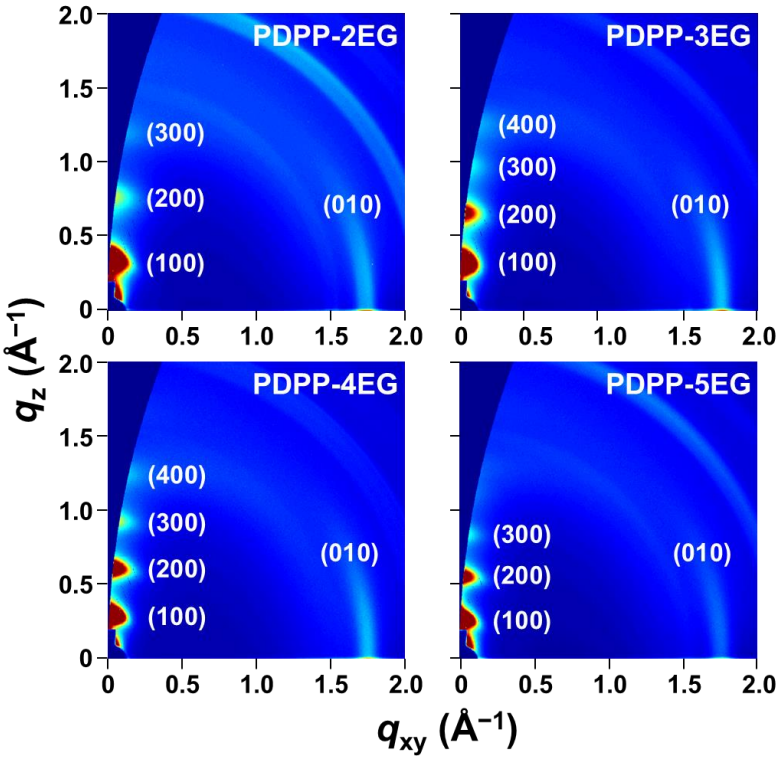

Figure S17. 2D GIXS images of the oxidized polymer films.

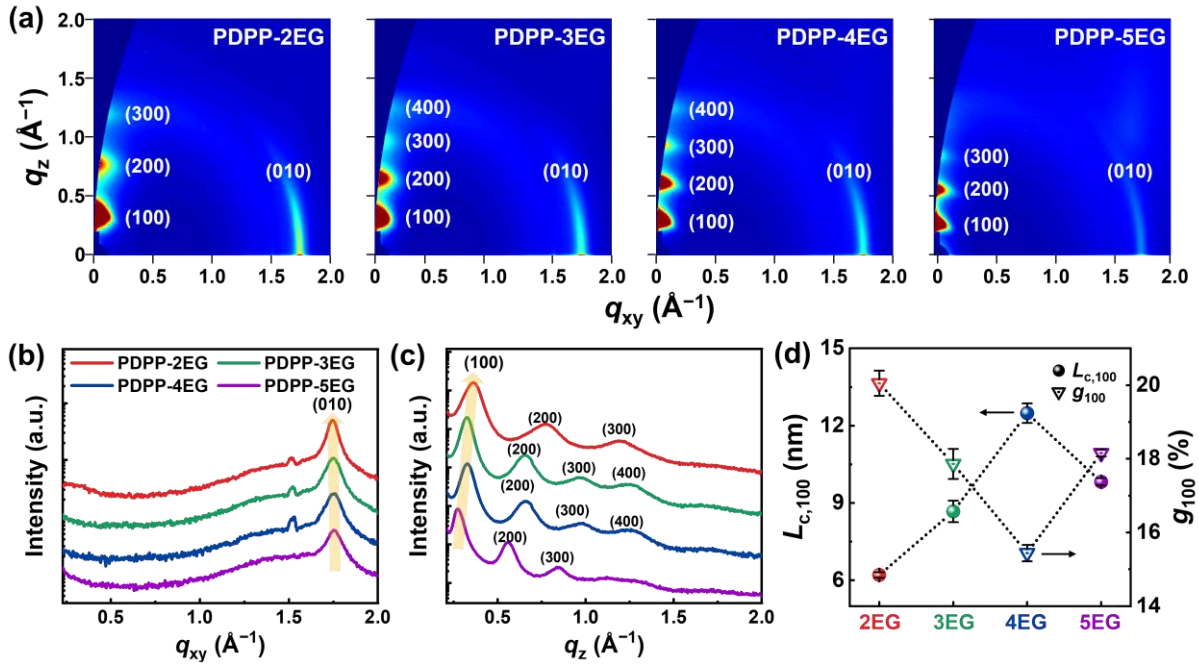

Figure S18. a) 2D GIXS images of the neat polymer films. The corresponding GIXS line-cut profiles in the b) in-plane and c) out-of-plane directions. d) Comparison of the coherence lengths and paracrystalline disorder parameters of (100) scattering peaks, which were averaged from at least three different films for each polymer.

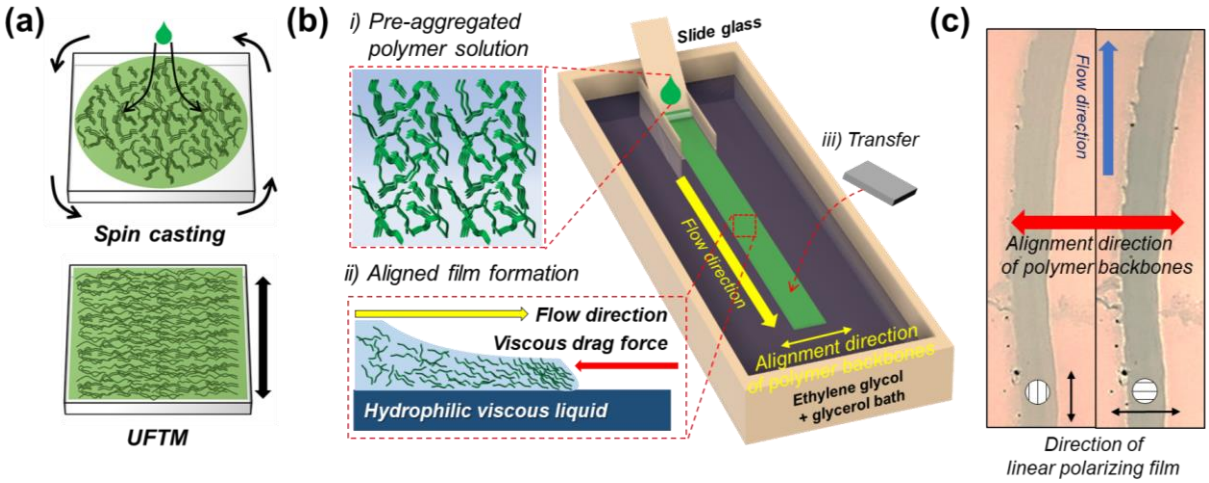

Figure S19. a) Schematics of overall polymer chain alignments in films prepared by spin-casting and UFTM. b) Schematics of the UFTM method. c) Photograph of floating films where a linear polarizing film is applied in the parallel and perpendicular directions to polymer backbone orientation.

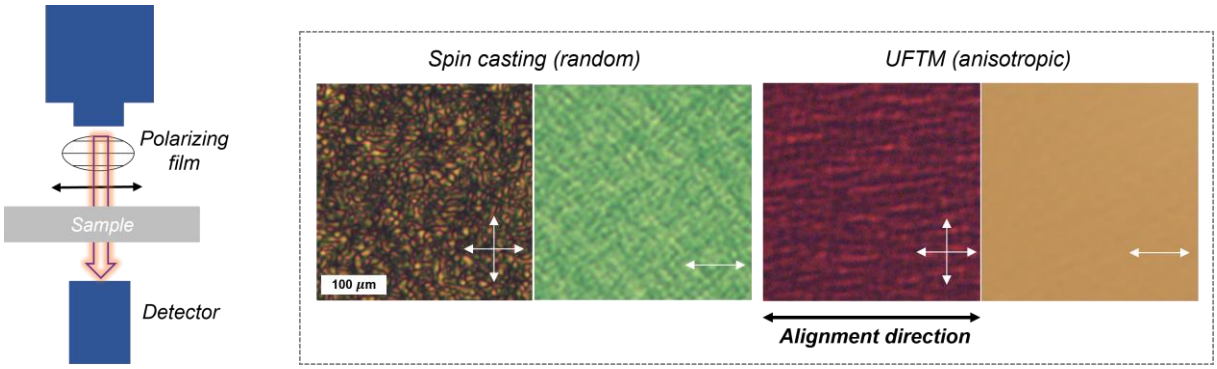

Figure S20. Cross-polarized OM images of spin-cast and UFTM films. The black arrow indicates the alignment direction of polymer backbones.

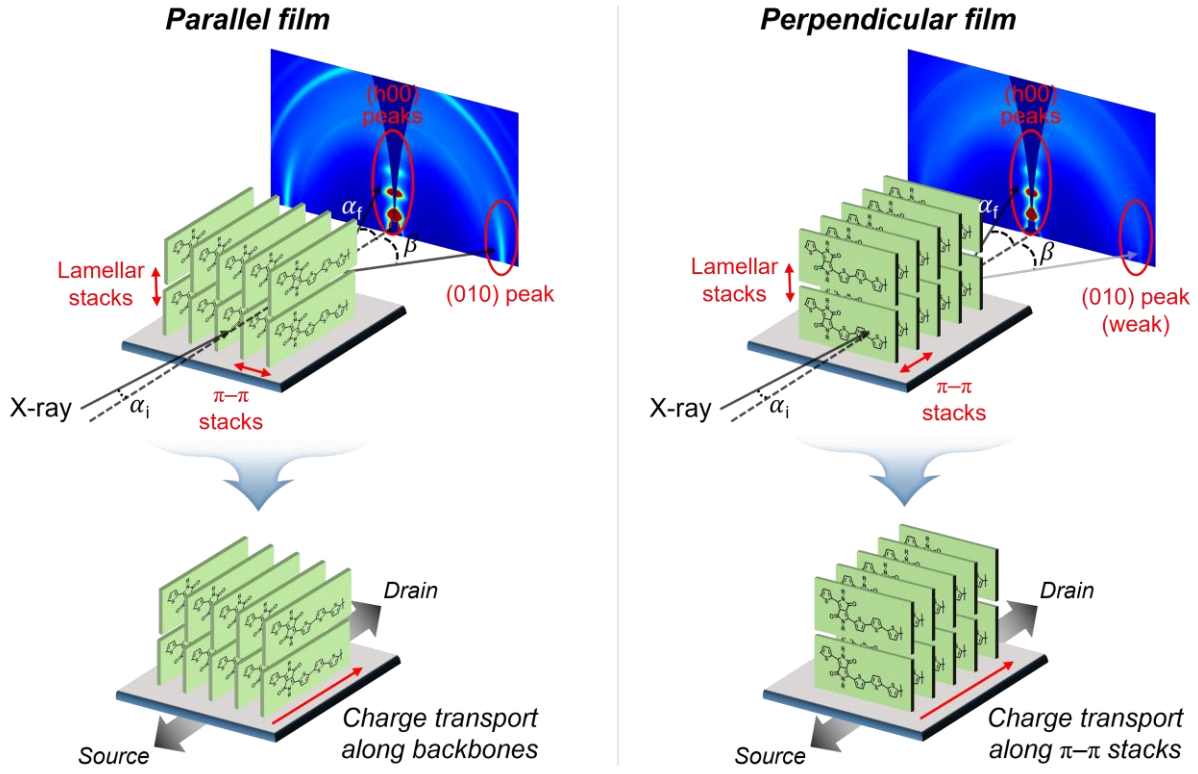

Figure S21. Schematics of polymer chain alignment during GIXS measurement and OECT fabrication. α_i: X-ray incident angle; α_f: exit angle; β: in-plane angle.

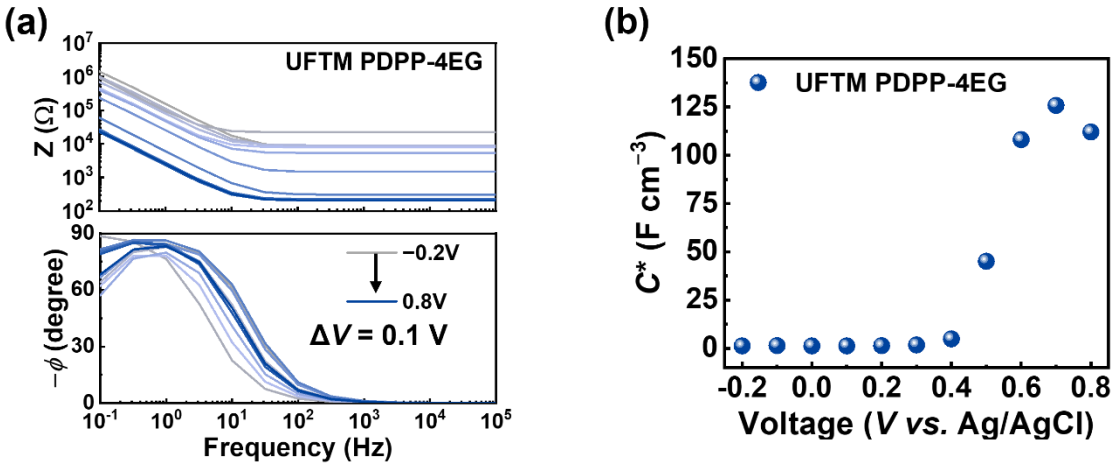

Figure S22. a) EIS curves for PDPP-4EG UFTM films at different offset DC voltages relative to the Ag/AgCl electrode. b) Volumetric capacitances of UFTM PDPP-4EG films extracted from EIS measurements as a function of the voltage of the working electrode.

Table S1. Performance metrics of *p*-type accumulation-mode OECTs based on liquid gate electrolytes.

Year	Active materials	μ_{OECT} [$cm^2 V^{-1} s^{-1}$]	C^* [$F cm^{-3}$]	[μC^*] [$F V^{-1} cm^{-1} s^{-1}$]	$\mu_{OECT} \times C^*$ [$F V^{-1} cm^{-1} s^{-1}$]	Electrolyte	Ref.
2014	PTHS+EG	1.3×10^{-3}	124	5.5	0.16	0.1M NaCl	[4]
2016	gBDT-g2T	0.018	77	4.8	1.4	0.1M NaCl	[5]
2016	g2T-T	0.28	220	167	62	0.1M NaCl	[5]
2016	p(g2T-TT)	1.27	241	261	227	0.1M NaCl	[6]
2018	$PTHS^-TBA^+$	8.18×10^{-9}	5	4.09×10^{-8}		0.1M NaCl	[7]
2018	$PTHS^-TEA^+$	8.21×10^{-9}	22	1.81×10^{-7}		0.1M NaCl	[7]
2018	$PTHS^-TMA^+$	2.67×10^{-11}	82	2.19×10^{-9}		0.1M NaCl	[7]
2018	$PTHS^-TBA^+$+EG	2.88×10^{-11}	15	4.32×10^{-10}		0.1M NaCl	[7]
2018	$PTHS^-TEA^+$+EG	5.37×10^{-8}	13	6.98×10^{-7}		0.1M NaCl	[7]
2018	gBDT-MeOT2		95			0.1M NaCl	[8]
2018	ProDOT(OE)-DMP	0.063	111	6.993		0.1M NaCl	[9]
2019	p(g2T-TT)			268		0.1M NaF	[10]
2019	p(g2T-TT)			271		0.1M NaCl	[10]
2019	p(g2T-TT)			381		0.1M NaBr	[10]
2019	p(g2T-TT)			393		0.1M $NaBF_4$	[10]
2019	p(g2T-TT)			458		0.1M $NaSBF_6$	[10]
2019	P3HT			10.4		0.1M KCl	[11]
2019	P3MEEMT	0.281	175	49.1		0.1M KCl	[11]
2019	P3MEEMT	0.329	294	96.7		0.1 KPF_6	[11]
2019	TFT-T			10		0.1M NaCl	[12]
2019	$PTHS^-TMA^+$		82			0.1M NaCl	[13]
2019	$PTHS^-TMA^+$-*co*-P3HT 1		107		0.97	0.1M NaCl	[13]
2019	$PTHS^-TMA^+$-*co*-P3HT 2		100		1.7	0.1M NaCl	[13]
2019	P3CPT		150			0.1M NaCl	[14]
2020	g-0%		19		0.001	0.1M NaCl	[15]
2020	g-50%		97		0.873	0.1M NaCl	[15]
2020	g-75%		206		78.28	0.1M NaCl	[15]
2020	g-100%		297		163.35	0.1M NaCl	[15]
2020	2g		231		16.17	0.1M NaCl	[15]
2020	P3MEET	5.2×10^{-4}	80	0.04		0.1M NaCl	[16]
2020	P3MEEMT	0.06	160	9.8		0.1M NaCl	[16]
2020	P3MEEET	0.05	242	11.5		0.1M NaCl	[16]
2020	p(gPyDPP-MeOT2)		60		1.8	0.1M NaCl	[17]
2020	PEDOT:PSS+DETA		53.6			0.1M NaCl	[18]
2020	PEDOT:PSS+DEMTA	2.17	50.4	109.368		0.1M NaCl	[18]
2020	PEDOT:PSS+TAEA		46.1			0.1M NaCl	[18]
2020	P4E4+PEO			0.81		0.1M NaCl	[19]
2020	PCPDTBT-SO_3K		134			0.1M NaCl	[20]
2020	p(g2T2-T)	$\sim 10^{-4}$	8	9		0.1M NaCl	[21]
2020	p(g3T2-T)	0.16	211	135		0.1M NaCl	[21]
2020	p(g4T2-T)	0.06	192	54		0.1M NaCl	[21]
2020	p(g3T2)	0.90	156	161		0.1M NaCl	[22]
2020	p(g2T2-g4T2)	1.72	187	522		0.1M NaCl	[22]
2020	p(g1T2-g5T2)	2.61	133	496		0.1M NaCl	[22]

2020	p(g0T2-g6T2)	2.95	74	302		0.1M NaCl	[22]
2021	PTDPP-DT	1.1	123	149		0.1M NaCl	[23]
2021	P3HHT	0.04		35		0.1M KCl	[24]
2021	p(gDPP-TT)	0.57	184	125		0.1M NaCl	[25]
2021	p(gDPP-T2)	1.55	196	342		0.1M NaCl	[25]
2021	p(gDPP-MeOT2)	0.28	169	57		0.1M NaCl	[25]
2021	p($g_4$2T-T)	0.39	258	86	100	0.1M NaCl	[26]
2021	p[p($g_4$2T-T)-*co*-U]	0.15	279	36	42	0.1M NaCl	[26]
2021	P(aDTDPP-bis-EDOT)	0.095	21.50	2.04		0.1M NaCl	[27]
2021	P(gDTDPP-bis-EDOT)	0.087	189.6	16.5		0.1M NaCl	[27]
2021	P(gDTDPP-aBT)	0.044	24.73	1.08		0.1M NaCl	[27]
2021	*p*-P3HT			347		0.1M KCl	[28]
2021	*d*-P3HT			147		0.1M KCl	[28]
2021	*p*-DPPDTT			62		0.1M KCl	[28]
2021	*d*-DPPDTT			49		0.1M KCl	[28]
2021	*p*-Pg2T-T			94		0.1M KCl	[28]
2021	*d*-Pg2T-T			78		0.1M KCl	[28]
2021	PDPP[T]$_2${TEG}-EDOT	0.084	167	14.1		0.1M NaCl	[29]
2021	PDPP[T]$_2${TEG}3-MEET	0.133	338	45.4		0.1M NaCl	[29]
2021	P(bgDPP-T)	1.59	3.7	6		0.1M NaCl	[30]
2021	P(bgDPP-T2)	0.50	84.1	42		0.1M NaCl	[30]
2021	P(lgDPP-MeOT2)	2.15	80.8	174		0.1M NaCl	[30]
2021	P(bgDPP-MeOT2)	1.63	120.0	195		0.1M NaCl	[30]
2021	p(g2T2)	0.03	187	5.0		0.1M NaCl	[31]
2021	p(g2T2-g3T2)	2.35	161	378		0.1M NaCl	[31]
2021	p(g3T2)	1.04	122	127		0.1M NaCl	[31]
2021	pgBTTT	3.44	164	502	563	0.1M NaCl	[32]
2021	p(g2T-TT)	0.41	244	93	90	0.1M NaCl	[32]
2021	PgBT(F)2gT	0.060	170	6.29		0.1M NaCl	[33]
2021	PgBT(F)2gTT	0.931	111	99.7		0.1M NaCl	[33]
2021	2DPP-OD-TEG	0.516	61.6	31.8		0.1M $NaClO_4$	[34]
2021	DPP-DTT+PS	7.28	7.1	123.4		0.1M KPF_6	[35]
2021	TDPP-gTVT	1.1	173.5	205.2		0.1M NaCl	[36]
2021	TDPP-gTBTT	0.18	122.5	21.5		0.1M NaCl	[36]
2022	p(g2T-TT)	1.82	171.4	299.42		0.1M NaCl	[37]
2022	p(p2T-TT)	1.76	103.21	182.24		0.1M NaCl	[37]
2022	p(b2T-TT)	3.03	113.93	342.2		0.1M NaCl	[37]
2022	PEDOT-Phos	2.83×10^{-5}	282	0.008		0.1M NaCl	[38]
2022	P3HT+PTEO			151		0.1M NaCl	[39]
2022	P3HT+PTEO-OH			13		0.1M NaCl	[39]
2022	P3gCPDT-2gT2	0.66	140	92.0		0.1M NaCl	[40]
2022	P3gCPDT-1gT2	0.90	320	288.6		0.1M NaCl	[40]
2022	P3gCPDT-MeOT2	3.10	145	448.6		0.1M NaCl	[40]
2022	IG-T	2.7×10^{-3}	76.2	0.20		0.1M NaCl	[41]
2022	TIG-T	1.1	121	132		0.1M NaCl	[41]
2022	TIG-BT	0.61	82.1	55		0.1M NaCl	[41]
2022	P3MEEMT	0.23	215.5	49.1		0.1M KCl	[42]
2022	P3APPT	0.38	81.0	30.5		0.1M KCl	[42]
2022	P3AAPT	0.36	25.4	9.2		0.1M KCl	[42]
2022	P3PAAT		1.3			0.1M KCl	[42]
2022	P3MEEMT	0.37	259	96.7		0.1M KPF_6	[42]
2022	P3APPT	0.27	152.0	41.3		0.1M KPF_6	[42]

2022	P3AAPT	0.20	167.2	33.2	0.1M KPF_6	[42]
2022	P3PAAT	0.16	84.0	13.3	0.1M KPF_6	[42]
2022	p(g2T-T)	~2.1	~180	~380	0.1M NaCl	[43]
2022	TIIP	0.05	32	1.75	0.1M NaCl	[44]
2022	p(g3T2-T)+BCF	3.35	166	556.31	0.1M NaCl	[45]
2022	PBBTL	0.034	143	4.82	0.1M NaCl	[46]
2022	PBBTL+BBL	0.022	124	2.72	0.1M NaCl	[46]
2022	$PrC_{60}MA$+p(g2T-TT)			22.8	0.1M KCl	[47]
2022	P(gTDPPT)	0.40	161	65.1	0.1M NaCl	[48]
2022	P(3HT-*co*-3HHT)	0.189	190	36	0.1M KCl	[49]
2022	P(3HT-*co*-3HHT)+P3HT-*b*-PEO	0.132	190	25	0.1M KCl	[49]
2023	G2-DMP	0.32	227	73	0.1M NaCl	[50]
2023	G3-DMP	0.26	214	57	0.1M NaCl	[50]
2023	G4-DMP	0.94	213	200	0.1M NaCl	[50]
2022	$p(g_4T2\text{-}TT)$	3.13	120	374	0.1M NaCl	[51]
2022	$p(g_4T2\text{-}TT)$ [a)]	6.53	308	2008	0.1M NaCl	[51]
2023	$Cu_3(HHTP)_2$	0.16	84.9	13.4	0.05M $CaCl_2$	[52]
2023	CPE-C2-Na		5.1		0.1M NaCl	[53]
2023	CPE-C3-Na		220		0.1M NaCl	[53]
2023	CPE-C4-Na		250		0.1M NaCl	[53]
2023	CPE-C5-Na		190		0.1M NaCl	[53]
2023	P3MEEET	0.14	219	31.4	0.1M NaCl	[54]
2023	P3MEEET	2.14	156	332	0.02M KTFSI	[54]
2023	PgBT(Ion)2gTT	1.02	143	145.33	0.1M NaCl	[55]
2023	PgBT(TriEG)2gTT	0.26	147	39.37	0.1M NaCl	[55]
2023	PgBT(F)2gTT	1.03	121	125.43	0.1M NaCl	[55]
2023	Nafion-P3HT	0.6	6.1	3.5	PBS	[56]
2023	g2T2-gBT2	0.18	224	40	0.1M NaCl	[57]
2023	g2T2-gBT4	0.99	364	359	0.1M NaCl	[57]
2023	g2T2-gBT6	0.47	435	203	0.1M NaCl	[57]
2023	inDTP-P	0.26	147	38	0.1M NaCl	[58]
2023	outDTP-P	0.61	113	69	0.1M NaCl	[58]
2023	inDTP-T	1.65	162	267	0.1M NaCl	[58]
2023	outDTP-T	0.38	117	45	0.1M NaCl	[58]
2023	inDTP-2T	0.68	168	115	0.1M NaCl	[58]
2023	outDTP-2T	0.39	166	65	0.1M NaCl	[58]
2023	p-Pg2T-T			354.6	PBS	[59]
2023	PDPP-2EG [b)]	0.21	97.89	20	0.1M NaCl	
2023	PDPP-3EG [b)]	4.32	113.58	491	0.1M NaCl	
2023	PDPP-4EG [b)]	6.52	107.72	702	0.1M NaCl	
2023	PDPP-5EG [b)]	3.20	107.88	346	0.1M NaCl	

[a)] The post-purified polymer batch was used by dividing one batch into several fractions with lower dispersity as well as removing residual palladium using a preparative gel permeation chromatography.
[b)] Developed in this work.

Table S2. Performance metrics of *n*-type accumulation-mode OECTs based on liquid gate electrolytes.

Year	Active materials [a)]	μ_{OECT} [$cm^2 V^{-1} s^{-1}$]	C^* [$F cm^{-3}$]	[μC^*] [$F V^{-1} cm^{-1} s^{-1}$]	$\mu_{OECT} \times C^*$ [$F V^{-1} cm^{-1} s^{-1}$]	Electrolyte	Ref.
2016	P(gNDI-gT2)	3.1×10^{-4}	397	0.18	0.12	0.1M NaCl	[60]
2016	P(gNDI-T2)		190			0.1M NaCl	[60]
2018	BBL	7×10^{-4}	930	0.651		0.1M NaCl	[61]
2018	P-75		188.0		0.027	0.1M NaCl	[62]
2018	P-90		198.2		0.047	0.1M NaCl	[62]
2018	P-100		192.4		0.038	0.1M NaCl	[62]
2019	P-90		317	0.054	0.059	0.1M NaCl	[63]
2019	C60-TEG	0.03	220	7.0		0.1M KCl	[64]
2019	P-90:PFBT	1.2×10^{-5}	61.9	0.0008		0.1M NaCl	[65]
2019	P-90:MBT	1.7×10^{-5}	132.5	0.0023		0.1M NaCl	[65]
2020	p(NDI-T2-L2)	3.26×10^{-3}	95	0.31		PBS	[66]
2020	P-90+TBAF		143			0.1M NaCl	[67]
2021	PgNaN	6.50×10^{-3}	100	0.662	0.652	0.1M NaCl	[68]
2021	PgNgN	1.89×10^{-4}	239	0.037	0.046	0.1M NaCl	[68]
2021	p(C_4-T2)	1.90×10^{-3}	158	0.30		0.1M NaCl	[69]
2021	p(C_4-T2-OMe)	3.87×10^{-4}	170	0.07		0.1M NaCl	[69]
2021	p(C_4-T2-C_0-EG)	1.16×10^{-3}	188	0.22		0.1M NaCl	[69]
2021	p(C_4-T2-C_2-EG)	4.99×10^{-5}	200	0.01		0.1M NaCl	[69]
2021	p(C_4-T2-C_4-EG)	5.34×10^{-5}	116	0.006		0.1M NaCl	[69]
2021	p(C_2-T2)	3.97×10^{-4}	492	0.20		0.1M NaCl	[69]
2021	p(C_4-T2)	1.90×10^{-3}	158	0.30		0.1M NaCl	[69]
2021	p(C_6-T2)	4.74×10^{-3}	272	1.29		0.1M NaCl	[69]
2021	p(C_8-T2)	3.76×10^{-4}	342	0.13		0.1M NaCl	[69]
2021	p(gNDI-gT2)	2.7×10^{-4}	221	0.06		0.1M NaCl	[70]
2021	p(C3-gNDI-gT2)	1.81×10^{-3}	72	0.13		0.1M NaCl	[70]
2021	p(C6-gNDI-gT2)	2.71×10^{-3}	59	0.16		0.1M NaCl	[70]
2021	BBL	2.14×10^{-3}	731	1.99	1.57	0.1M NaCl	[71]
2021	P-90	7.45×10^{-5}	261.5	0.0343	0.0195	0.1M NaCl	[71]
2021	2DPP-OD-TEG	0.0465	146.2	6.8		0.1M $NaClO_4$	[34]
2021	f-BTI2TEG-T	0.044	52	2.30		0.1M NaCl	[72]
2021	f-BTI2TEG-FT	0.034	443	15.20		0.1M NaCl	[72]
2021	p([75:25]NDI-g3T2)			0.023		0.1M NaCl	[73]
2021	p([90:10]NDI-g3T2)			0.046		0.1M NaCl	[73]
2021	p([100:0]NDI-g3T2)			0.012		0.1M NaCl	[73]
2021	p([90:10]NDI-T2)			0.04		0.1M NaCl	[73]
2021	p([100:0]NDI-T2)			0.04		0.1M NaCl	[73]
2022	BBL_{15}	3.59×10^{-3}	540	1.94		0.1M NaCl	[74]
2022	BBL_{60}	9.42×10^{-3}	520	4.90		0.1M NaCl	[74]
2022	BBL_{98}	0.0205	499	10.2		0.1M NaCl	[74]
2022	BBL_{152}	0.0440	589	25.9		0.1M NaCl	[74]
2022	p(C-T)	0.069	97	6.7		0.1M NaCl	[75]
2022	p(N-T)	0.059	73	4.3		0.1M NaCl	[75]
2022	p(C-2T)	0.019	53	1.0		0.1M NaCl	[75]
2022	P(NDITEG-T)	2.4×10^{-3}	165.8	0.04		0.1M NaCl	[76]
2022	P(NDIDTEG-T)	9.4×10^{-3}	221.5	0.21		0.1M NaCl	[76]
2022	P(NDIDEG-T)	0.0212	239.9	0.51		0.1M NaCl	[76]
2022	P(NDIMTEG-T)	0.0223	250.9	0.56		0.1M NaCl	[76]
2022	P(gPzDPP-2T)	1.6×10^{-3}	134	0.22		0.1M NaCl	[77]

2022	P(gPzDPP-CT2)	0.019	91	1.72	0.1M NaCl	[77]
2022	AIG-BT	1.4×10^{-3}	83.5	0.12	0.1M NaCl	[41]
2022	p(g_7NC_2N)	2.00×10^{-3}	180	0.36	0.1M NaCl	[78]
2022	p(g_7NC_4N)	1.46×10^{-3}	126	0.18	0.1M NaCl	[78]
2022	p(g_7NC_6N)	2.29×10^{-3}	150	0.34	0.1M NaCl	[78]
2022	p(g_7NC_8N)	6.01×10^{-3}	199	1.19	0.1M NaCl	[78]
2022	p($g_7NC_{10}N$)	0.0120	153	1.83	0.1M NaCl	[78]
2022	p($g_7NC_{12}N$)	6.50×10^{-3}	100	0.66	0.1M NaCl	[78]
2022	p($g_7NC_{16}N$)	3.80×10^{-3}	86	0.33	0.1M NaCl	[78]
2022	4Cl-PDI-4EG	4.18×10^{-4}	303	0.13	0.1M NaCl	[79]
2022	4Cl-PDI-3EG	8.07×10^{-4}	198	0.17	0.1M NaCl	[79]
2022	PDI-3EG	3.79×10^{-4}	207	0.08	0.1M NaCl	[79]
2022	PNDI2TEG-2Tz	3.16×10^{-3}	367	1.16	0.1M NaCl	[80]
2022	gNDI-EDBT	3.96×10^{-4}	50.5	0.02	0.1M NaCl	[81]
2022	gNDI-BT	5.69×10^{-4}	158.3	0.09	0.1M NaCl	[81]
2022	gNDI-FBT	6.10×10^{-4}	196.6	0.12	0.1M NaCl	[81]
2022	f-BTI2g-TVT	0.014	110	1.50	0.1M NaCl	[82]
2022	f-BTI2g-TVTCN	0.24	170	41.3	0.1M NaCl	[82]
2022	gNR	0.013	198	2.5	0.1M NaCl	[83]
2022	hgNR	0.009	129	1.2	0.1M NaCl	[83]
2022	PBBTL+BBL	0.008	168	1.36	0.1M NaCl	[46]
2022	gNR	0.0178	288	5.12	0.1M NaCl	[84]
2022	4Cl-PDI-4EG	5.18×10^{-4}	367	0.19	0.1M NaCl	[84]
2022	$PrC_{60}MA$+p(g2T-TT)			11.8	0.1M KCl	[47]
2022	P4gNDI	7.34×10^{-6}	219	0.00161	0.1M NaCl	[85]
2022	P4gNDTI	1.42×10^{-3}	167	0.27	0.1M NaCl	[85]
2022	P(gTDPP2FT)	0.35	156	54.8	0.1M NaCl	[48]
2023	3gDNR	0.043	217	9.4	0.1M NaCl	[86]
2023	4gDNR	0.021	225	4.7	0.1M NaCl	[86]
2023	gNDI-V	0.014	144	2.31	0.1M KCl	[87]
2023	gNDI-T	0.0015	237	0.42	0.1M KCl	[87]
2023	p(C_6g_3NDI-T)	1.02×10^{-3}	222	0.227	0.1M NaCl	[51]
2023	gAIID-T	0.002	43.0	0.09	0.1M NaCl	[88]
2023	gAIID-2FT	0.049	99.8	4.09	0.1M NaCl	[88]
2023	BBL_H	9.2	1007.1	9.27	0.1M KCl	[89]
2023	BBL_L	0.52	539.8	0.28	0.1M KCl	[89]
2023	$Cu_3(HHTP)_2$	0.30	67.8	20.3	0.05M $CaCl_2$	[52]
2023	gNDI-Br2	6.4×10^{-4}	203.2	0.13	0.1M NaCl	[90]
2023	TDPP-CN-G7	0.005	165.2	0.80	0.1M NaCl	[91]
2023	TDPP-RD-G7	0.075	78.6	5.88	0.1M NaCl	[91]
2023	t-gdiPDI	8.3×10^{-4}	254	0.21	0.1M NaCl	[92]
2023	d-gdiPDI	5.3×10^{-4}	628	0.33	0.1M NaCl	[92]
2023	lgTNR	0.03	141	4.2	0.1M NaCl	[93]
2023	bgTNR	0.29	106	31.6	0.1M NaCl	[93]
2023	poly(DPP-TPD)	0.11	68.58	8.05	0.1M KCl	[94]

[a)] For a fair comparison of intrinsic material properties, mechanically engineered active channels or molecular weight-fractionated polymers are excluded.

Table S3. Performance metrics of depletion-mode OECTs based on liquid gate electrolytes.

Year	Active materials [a]	μ_{OECT} [$cm^2 V^{-1} s^{-1}$]	C^* [$F cm^{-3}$]	[μC^*] [$F V^{-1} cm^{-1} s^{-1}$]	$\mu_{OECT} \times C^*$ [$F V^{-1} cm^{-1} s^{-1}$]	Electrolyte	Ref.
2015	PEDOT:PSS		39.3			0.1M NaCl	[95]
2016	PEDOT:PSTFSILi100	0.23	26	20	6.1	0.1M NaCl	[96]
2016	PEDOT:PMATFSILi80	0.0024	27	0.15	0.06	0.1M NaCl	[96]
2016	PEDOT:PSS+5% EG	1.9	39	47	75	0.1M NaCl	[97]
2018	EG-P	3.226	31	100		0.1M NaCl	[98]
2018	Crys-P	4.336	113	490		0.1M NaCl	[98]
2019	PEDOT:PSS+[EMIM][TCM]	3.8	87	335		0.1M NaCl	[99]
2019	PEDOT:PSS (PSPT)	0.437				0.1M NaCl	[100]
2020	pEDOT:ClO_4		102			0.01M PBS	[101]
2020	pEDOTOH:ClO_4		227			0.01M PBS	[101]
2020	p(EDOT-*ran*-EDOTOH):ClO_4		153			0.01M PBS	[101]
2020	PEDOT:PSS+GOPS	0.016				PBS+0.1M NaCl	[102]
2020	PEDOT:PSS+[EMIM][Cl]	2.26	37.3	84		0.1M NaCl	[103]
2020	PEDOT:PSS+Triton X	2.4	38	91		0.1M NaCl	[104]
2020	PEGDA:PEDOT		1.28			0.1M NaCl	[105]
2020	P(Py:BPDSA:Py)-0		51			0.1M NaCl	[106]
2020	P(Py:BPDSA:Py)-25		85			0.1M NaCl	[106]
2020	P(Py:BPDSA:Py)-50		678			0.1M NaCl	[106]
2020	P(Py:BPDSA:Py)-75		663			0.1M NaCl	[106]
2020	P(Py:BPDSA:Py)-100		672			0.1M NaCl	[106]
2021	SA-PEDOT:PSS microfiber	12.86	122.2	1500		0.1M NaCl	[107]
2021	ACE-PEDOT:PSS microfiber	7.34	63.9	445		0.1M NaCl	[107]
2021	PEDOT:PSS+EMIM Cl			235		0.1M NaCl	[108]
2021	PEDOT:PSS+EMIM OTF	4.538	78	354		0.1M NaCl	[108]
2021	PEDOT:PSS+EMIM TFSI			314		0.1M NaCl	[108]
2021	PEDOT:PSS+EMIM TCM	4.787	89	426		0.1M NaCl	[108]
2022	PEDOT:PSS+GOPS (acetone)	1.083	~48	52		0.1M KCl	[109]
2022	PEDOT:PSS+GOPS (NMP)			47		0.1M KCl	[109]
2022	PEDOT:PSS+GOPS (DMSO)			56		0.1M KCl	[109]
2022	PEDOT:PSS (DMSO)	3.333	~48	160		0.1M KCl	[109]
2022	PEDOT:PSS+[EMIM][PF6]+DBSA	38.281	12.8	490		PBS	[110]
2022	PSS 33k-1.1	1.17	41	31.7		0.1 M KCl	[111]
2022	PSS 145k-1.1	0.92	48	32.2		0.1 M KCl	[111]
2022	PSS 144k-1.7	5.16	31	142.4		0.1 M KCl	[111]
2022	PEDOT:PSS+PBA		2.4		1.3	PBS	[112]
2022	PEDOT:PSS+15-crown-5	4.895	76	372		0.1M NaCl	[113]
2022	PEDOT:PSS+[MTEOA][$MeOSO_3$]	3.741	75.87	283.80		0.1M NaCl	[114]
2022	PBFDO [b]			180		0.1M NaCl	[115]
2022	PEDOT:PSS+PVA	2.6	83	252		0.1M NaCl	[116]
2022	Br2-P			27.1		0.1M NaCl	[117]
2022	Br5-P			6.12		0.1M NaCl	[117]
2022	TFSI5-P			50.7		0.1M NaCl	[117]
2022	PEDOT-N_3		226			PBS	[118]
2023	Nafion-PEDOT:PSS	21	7.8	166		PBS	[56]
2023	H_2SO_4-treated PEDOT:DBSA			55.6		NaCl	[119]

[a] For a fair comparison of intrinsic material properties, mechanically engineered active channels or molecular weight-fractionated polymers are excluded. [b] *n*-Type material.

Table S4. Coherence lengths and paracrystalline disorder parameters extracted from (010) scattering peaks in the GIXS results of the oxidized polymer films.

Polymer	$L_{c,010}$ [a)] [nm]	g_{010} [%]
PDPP-2EG	4.8 ± 0.3	10.4 ± 0.3
PDPP-3EG	4.9 ± 0.1	10.2 ± 0.2
PDPP-4EG	5.1 ± 0.3	10.2 ± 0.3
PDPP-5EG	5.2 ± 0.1	10.0 ± 0.1

[a)]Averaged over at least three oxidized films for each polymer.

References

[1] Y. Li, O. Sachnik, B. van der Zee, K. Thakur, C. Ramanan, G.-J. A. H. Wetzelaer, P. W. M. Blom, *Adv. Opt. Mater.* **2021**, *9*, 2101149.
[2] P. de Bruyn, A. H. P. van Rest, G. A. H. Wetzelaer, D. M. de Leeuw, P. W. M. Blom, *Phys. Rev. Lett.* **2013**, *111*, 186801.
[3] S. S. Hegedus, E. A. Fagen, *J. Appl. Phys.* **1992**, *71*, 5941.
[4] S. Inal, J. Rivnay, P. Leleux, M. Ferro, M. Ramuz, J. C. Brendel, M. M. Schmidt, M. Thelakkat, G. G. Malliaras, *Adv. Mater.* **2014**, *26*, 7450.
[5] C. B. Nielsen, A. Giovannitti, D.-T. Sbircea, E. Bandiello, M. R. Niazi, D. A. Hanifi, M. Sessolo, A. Amassian, G. G. Malliaras, J. Rivnay, I. McCulloch, *J. Am. Chem. Soc.* **2016**, *138*, 10252.
[6] A. Giovannitti, D.-T. Sbircea, S. Inal, C. B. Nielsen, E. Bandiello, D. A. Hanifi, M. Sessolo, G. G. Malliaras, I. McCulloch, J. Rivnay, *Proc. Natl. Acad. Sci. U.S.A.* **2016**, *113*, 12017.
[7] M. M. Schmidt, M. ElMahmoudy, G. G. Malliaras, S. Inal, M. Thelakkat, *Macromol. Chem. Phys.* **2018**, *219*, 1700374.
[8] A. Giovannitti, K. J. Thorley, C. B. Nielsen, J. Li, M. J. Donahue, G. G. Malliaras, J. Rivnay, I. McCulloch, *Adv. Funct. Mater.* **2018**, *28*, 1706325.
[9] L. R. Savagian, A. M. Österholm, J. F. Ponder Jr., K. J. Barth, J. Rivnay, J. R. Reynolds, *Adv. Mater.* **2018**, *30*, 1804647.
[10] C. Cendra, A. Giovannitti, A. Savva, V. Venkatraman, I. McCulloch, A. Salleo, S. Inal, J. Rivnay, *Adv. Funct. Mater.* **2019**, *29*, 1807034.
[11] L. Q. Flagg, C. G. Bischak, J. W. Onorato, R. B. Rashid, C. K. Luscombe, D. S. Ginger, *J. Am. Chem. Soc.* **2019**, *141*, 4345.
[12] Z. S. Parr, R. Halaksa, P. A. Finn, R. B. Rashid, A. Kovalenko, M. Weiter, J. Rivnay, J. Krajčovič, C. B. Nielsen, *ChemPlusChem* **2019**, *84*, 1384.
[13] P. Schmode, D. Ohayon, P. M. Reichstein, A. Savva, S. Inal, M. Thelakkat, *Chem. Mater.* **2019**, *31*, 5286.
[14] B. V. Khau, L. R. Savagian, M. De Keersmaecker, M. A. Gonzalez, E. Reichmanis, *ACS Mater. Lett.* **2019**, *1*, 599.
[15] A. Savva, R. Hallani, C. Cendra, J. Surgailis, T. C. Hidalgo, S. Wustoni, R. Sheelamanthula, X. Chen, M. Kirkus, A. Giovannitti, A. Salleo, I. McCulloch, S. Inal, *Adv. Funct. Mater.* **2020**, *30*, 1907657.
[16] P. Schmode, A. Savva, R. Kahl, D. Ohayon, F. Meichsner, O. Dolynchuk, T. Thurn-Albrecht, S. Inal, M. Thelakkat, *ACS Appl. Mater. Interfaces* **2020**, *12*, 13029.
[17] A. Giovannitti, R. B. Rashid, Q. Thiburce, B. D. Paulsen, C. Cendra, K. Thorley, D. Moia, J. T. Mefford, D. Hanifi, D. Weiyuan, M. Moser, A. Salleo, J. Nelson, I. McCulloch, J. Rivnay, *Adv. Mater.* **2020**, *32*, 1908047.
[18] S. T. Keene, T. P. A. van der Pol, D. Zakhidov, C. H. L. Weijtens, R. A. J. Janssen, A. Salleo, Y. van de Burgt, *Adv. Mater.* **2020**, *32*, 2000270.
[19] Z. S. Parr, R. B. Rashid, B. D. Paulsen, B. Poggi, E. Tan, M. Freeley, M. Palma, I. Abrahams, J. Rivnay, C. B. Nielsen, *Adv. Electron. Mater.* **2020**, *6*, 2000215.
[20] A. T. Lill, D. X. Cao, M. Schrock, J. Vollbrecht, J. Huang, T. Nguyen-Dang, V. V. Brus, B. Yurash, D. Leifert, G. C. Bazan, T.-Q. Nguyen, *Adv. Mater.* **2020**, *32*, 1908120.
[21] M. Moser, L. R. Savagian, A. Savva, M. Matta, J. F. Ponder, T. C. Hidalgo, D. Ohayon, R. Hallani, M. Reisjalali, A. Troisi, A. Wadsworth, J. R. Reynolds, S. Inal, I. McCulloch, *Chem. Mater.* **2020**, *32*, 6618.
[22] M. Moser, T. C. Hidalgo, J. Surgailis, J. Gladisch, S. Ghosh, R. Sheelamanthula, Q. Thiburce, A. Giovannitti, A. Salleo, N. Gasparini, A. Wadsworth, I. Zozoulenko, M. Berggren,

E. Stavrinidou, S. Inal, I. McCulloch, *Adv. Mater.* **2020**, *32*, 2002748.
[23] X. Wu, Q. Liu, A. Surendran, S. E. Bottle, P. Sonar, W. L. Leong, *Adv. Electron. Mater.* **2021**, *7*, 2000701.
[24] T. Nicolini, J. Surgailis, A. Savva, A. D. Scaccabarozzi, R. Nakar, D. Thuau, G. Wantz, L. J. Richter, O. Dautel, G. Hadziioannou, N. Stingelin, *Adv. Mater.* **2021**, *33*, 2005723.
[25] M. Moser, A. Savva, K. Thorley, B. D. Paulsen, T. C. Hidalgo, D. Ohayon, H. Chen, A. Giovannitti, A. Marks, N. Gasparini, A. Wadsworth, J. Rivnay, S. Inal, I. McCulloch, *Angew. Chem. Int. Ed.* **2021**, *60*, 7777.
[26] S. Zokaei, R. Kroon, J. Gladisch, B. D. Paulsen, W. Sohn, A. I. Hofmann, G. Persson, A. Stamm, P.-O. Syrén, E. Olsson, J. Rivnay, E. Stavrinidou, A. Lund, C. Müller, *Adv. Sci.* **2021**, *8*, 2002778.
[27] N. Wang, L. Xie, H. Ling, V. Piradi, L. Li, X. Wang, X. Zhu, F. Yan, *J. Mater. Chem. C* **2021**, *9*, 4260.
[28] L. Huang, Z. Wang, J. Chen, B. Wang, Y. Chen, W. Huang, L. Chi, T. J. Marks, A. Facchetti, *Adv. Mater.* **2021**, *33*, 2007041.
[29] G. Krauss, F. Meichsner, A. Hochgesang, J. Mohanraj, S. Salehi, P. Schmode, M. Thelakkat, *Adv. Funct. Mater.* **2021**, *31*, 2010048.
[30] H. Jia, Z. Huang, P. Li, S. Zhang, Y. Wang, J.-Y. Wang, X. Gu, T. Lei, *J. Mater. Chem. C* **2021**, *9*, 4927.
[31] M. Moser, J. Gladisch, S. Ghosh, T. C. Hidalgo, J. F. Ponder Jr., R. Sheelamanthula, Q. Thiburce, N. Gasparini, A. Wadsworth, A. Salleo, S. Inal, M. Berggren, I. Zozoulenko, E. Stavrinidou, I. McCulloch, *Adv. Funct. Mater.* **2021**, *31*, 2100723.
[32] R. K. Hallani, B. D. Paulsen, A. J. Petty, R. Sheelamanthula, M. Moser, K. J. Thorley, W. Sohn, R. B. Rashid, A. Savva, S. Moro, J. P. Parker, O. Drury, M. Alsufyani, M. Neophytou, J. Kosco, S. Inal, G. Costantini, J. Rivnay, I. McCulloch, *J. Am. Chem. Soc.* **2021**, *143*, 11007.
[33] B. Ding, G. Kim, Y. Kim, F. D. Eisner, E. Gutiérrez-Fernández, J. Martín, M.-H. Yoon, M. Heeney, *Angew. Chem. Int. Ed.* **2021**, *60*, 19679.
[34] J. J. Samuel, A. Garudapalli, A. A. Mohapatra, C. Gangadharappa, S. Patil, N. P. B. Aetukuri, *Adv. Funct. Mater.* **2021**, *31*, 2102903.
[35] R. Giridharagopal, J. Guo, J. Kong, D. S. Ginger, *ACS Appl. Mater. Interfaces* **2021**, *13*, 34616.
[36] Y. Wang, A. Hamidi-Sakr, J. Surgailis, Y. Zhou, H. Liao, J. Chen, G. Zhu, Z. Li, S. Inal, W. Yue, *J. Mater. Chem. C* **2021**, *9*, 13338.
[37] M. Moser, Y. Wang, T. C. Hidalgo, H. Liao, Y. Yu, J. Chen, J. Duan, F. Moruzzi, S. Griggs, A. Marks, N. Gasparini, A. Wadsworth, S. Inal, I. McCulloch, W. Yue, *Mater. Horiz.* **2022**, *9*, 973.
[38] J. Hopkins, K. Fidanovski, L. Travaglini, D. Ta, J. Hook, P. Wagner, K. Wagner, A. Lauto, C. Cazorla, D. Officer, D. Mawad, *Chem. Mater.* **2022**, *34*, 140.
[39] H. J. Kim, K. Perera, Z. Liang, B. Bowen, J. Mei, B. W. Boudouris, *ACS Macro Letters* **2022**, *11*, 243.
[40] L. Lan, J. Chen, Y. Wang, P. Li, Y. Yu, G. Zhu, Z. Li, T. Lei, W. Yue, I. McCulloch, *Chem. Mater.* **2022**, *34*, 1666.
[41] Z. S. Parr, J. Borges-González, R. B. Rashid, K. J. Thorley, D. Meli, B. D. Paulsen, J. Strzalka, J. Rivnay, C. B. Nielsen, *Adv. Mater.* **2022**, *34*, 2107829.
[42] S. E. Chen, L. Q. Flagg, J. W. Onorato, L. J. Richter, J. Guo, C. K. Luscombe, D. S. Ginger, *J. Mater. Chem. A* **2022**, *10*, 10738.
[43] Y. Dai, S. Dai, N. Li, Y. Li, M. Moser, J. Strzalka, A. Prominski, Y. Liu, Q. Zhang, S.

Li, H. Hu, W. Liu, S. Chatterji, P. Cheng, B. Tian, I. McCulloch, J. Xu, S. Wang, *Adv. Mater.* **2022**, *34*, 2201178.
[44] R. B. Rashid, A. M. Evans, L. A. Hall, R. R. Dasari, E. K. Roesner, S. R. Marder, D. M. D'Allesandro, W. R. Dichtel, J. Rivnay, *Adv. Mater.* **2022**, *34*, 2110703.
[45] T. C. Hidalgo Castillo, M. Moser, C. Cendra, P. D. Nayak, A. Salleo, I. McCulloch, S. Inal, *Chem. Mater.* **2022**, *34*, 6723.
[46] X. Wu, T. L. D. Tam, S. Chen, T. Salim, X. Zhao, Z. Zhou, M. Lin, J. Xu, Y.-L. Loo, W. L. Leong, *Adv. Mater.* **2022**, *34*, 2206118.
[47] E. Stein, O. Nahor, M. Stolov, V. Freger, I. M. Petruta, I. McCulloch, G. L. Frey, *Nat. Commun.* **2022**, *13*, 5548.
[48] P. Li, J. Shi, Y. Lei, Z. Huang, T. Lei, *Nat. Commun.* **2022**, *13*, 5970.
[49] M. Barker, T. Nicolini, Y. A. Yaman, D. Thuau, O. Siscan, S. Ramachandran, E. Cloutet, C. Brochon, L. J. Richter, O. J. Dautel, G. Hadziioannou, N. Stingelin, *Mater. Horiz.* **2023**, *10*, 248.
[50] B. T. DiTullio, L. R. Savagian, O. Bardagot, M. De Keersmaecker, A. M. Österholm, N. Banerji, J. R. Reynolds, *J. Am. Chem. Soc.* **2023**, *145*, 122.
[51] S. Griggs, A. Marks, D. Meli, G. Rebetez, O. Bardagot, B. D. Paulsen, H. Chen, K. Weaver, M. I. Nugraha, E. A. Schafer, J. Tropp, C. M. Aitchison, T. D. Anthopoulos, N. Banerji, J. Rivnay, I. McCulloch, *Nat. Commun.* **2022**, *13*, 7964.
[52] J. Song, H. Liu, Z. Zhao, X. Guo, C.-k. Liu, S. Griggs, A. Marks, Y. Zhu, H. K.-w. Law, I. McCulloch, F. Yan, *Sci. Adv.* **2023**, *9*, eadd9627.
[53] L. C. Llanes, A. T. Lill, Y. Wan, S. Chae, A. Yi, T. Nguyen-Dang, H. J. Kim, L. Sepunaru, J. Read de Alaniz, G. Lu, G. C. Bazan, T.-Q. Nguyen, *J. Mater. Chem. C* **2023**, *11*, 8274.
[54] J. Tropp, D. Meli, R. Wu, B. Xu, S. B. Hunt, J. D. Azoulay, B. D. Paulsen, J. Rivnay, *ACS Mater. Lett.* **2023**, *5*, 1367.
[55] B. Ding, I.-Y. Jo, H. Yu, J. H. Kim, A. V. Marsh, E. Gutiérrez-Fernández, N. Ramos, C. L. Rapley, M. Rimmele, Q. He, J. Martín, N. Gasparini, J. Nelson, M.-H. Yoon, M. Heeney, *Chem. Mater.* **2023**, *35*, 3290.
[56] L. Zhang, S. Khayour, G. Ren, S. He, J. Wang, L. Yu, Y. Song, C. Zhu, X. Kang, Y. Zhang, Z. Gong, K. Gao, J. Wang, H. Sheng, G. Lu, H.-D. Yu, *J. Mater. Chem. C* **2023**, *11*, 7272.
[57] S. Cong, J. Chen, B. Ding, L. Lan, Y. Wang, C. Chen, Z. Li, M. Heeney, W. Yue, *Mater. Horiz.* **2023**, DOI: 10.1039/D3MH00418J.
[58] R. Halaksa, J. H. Kim, K. J. Thorley, P. A. Gilhooly-Finn, H. Ahn, A. Savva, M.-H. Yoon, C. B. Nielsen, *Angew. Chem. Int. Ed.* **2023**, *62*, e202304390.
[59] C. Liu, J. Deng, L. Gao, J. Cheng, Y. Peng, H. Zeng, W. Huang, L.-W. Feng, J. Yu, *Adv. Electron. Mater.* **2023**, *9*, 2300119.
[60] A. Giovannitti, C. B. Nielsen, D.-T. Sbircea, S. Inal, M. Donahue, M. R. Niazi, D. A. Hanifi, A. Amassian, G. G. Malliaras, J. Rivnay, I. McCulloch, *Nat. Commun.* **2016**, *7*, 13066.
[61] H. Sun, M. Vagin, S. Wang, X. Crispin, R. Forchheimer, M. Berggren, S. Fabiano, *Adv. Mater.* **2018**, *30*, 1704916.
[62] A. Giovannitti, I. P. Maria, D. Hanifi, M. J. Donahue, D. Bryant, K. J. Barth, B. E. Makdah, A. Savva, D. Moia, M. Zetek, P. R. F. Barnes, O. G. Reid, S. Inal, G. Rumbles, G. G. Malliaras, J. Nelson, J. Rivnay, I. McCulloch, *Chem. Mater.* **2018**, *30*, 2945.
[63] A. Savva, D. Ohayon, J. Surgailis, A. F. Paterson, T. C. Hidalgo, X. Chen, I. P. Maria, B. D. Paulsen, A. J. Petty II, J. Rivnay, I. McCulloch, S. Inal, *Adv. Electron. Mater.* **2019**, *5*, 1900249.
[64] C. G. Bischak, L. Q. Flagg, K. Yan, C.-Z. Li, D. S. Ginger, *ACS Appl. Mater.*

Interfaces **2019**, *11*, 28138.
[65] A. F. Paterson, H. Faber, A. Savva, G. Nikiforidis, M. Gedda, T. C. Hidalgo, X. Chen, I. McCulloch, T. D. Anthopoulos, S. Inal, *Adv. Mater.* **2019**, *31*, 1902291.
[66] M. Kawan, T. C. Hidalgo, W. Du, A.-M. Pappa, R. M. Owens, I. McCulloch, S. Inal, *Mater. Horiz.* **2020**, *7*, 2348.
[67] A. F. Paterson, A. Savva, S. Wustoni, L. Tsetseris, B. D. Paulsen, H. Faber, A. H. Emwas, X. Chen, G. Nikiforidis, T. C. Hidalgo, M. Moser, I. P. Maria, J. Rivnay, I. McCulloch, T. D. Anthopoulos, S. Inal, *Nat. Commun.* **2020**, *11*, 3004.
[68] X. Chen, A. Marks, B. D. Paulsen, R. Wu, R. B. Rashid, H. Chen, M. Alsufyani, J. Rivnay, I. McCulloch, *Angew. Chem. Int. Ed.* **2021**, *60*, 9368.
[69] D. Ohayon, A. Savva, W. Du, B. D. Paulsen, I. Uguz, R. S. Ashraf, J. Rivnay, I. McCulloch, S. Inal, *ACS Appl. Mater. Interfaces* **2021**, *13*, 4253.
[70] I. P. Maria, B. D. Paulsen, A. Savva, D. Ohayon, R. Wu, R. Hallani, A. Basu, W. Du, T. D. Anthopoulos, S. Inal, J. Rivnay, I. McCulloch, A. Giovannitti, *Adv. Funct. Mater.* **2021**, *31*, 2008718.
[71] J. Surgailis, A. Savva, V. Druet, B. D. Paulsen, R. Wu, A. Hamidi-Sakr, D. Ohayon, G. Nikiforidis, X. Chen, I. McCulloch, J. Rivnay, S. Inal, *Adv. Funct. Mater.* **2021**, *31*, 2010165.
[72] K. Feng, W. Shan, S. Ma, Z. Wu, J. Chen, H. Guo, B. Liu, J. Wang, B. Li, H. Y. Woo, S. Fabiano, W. Huang, X. Guo, *Angew. Chem. Int. Ed.* **2021**, *60*, 24198.
[73] A. A. Szumska, I. P. Maria, L. Q. Flagg, A. Savva, J. Surgailis, B. D. Paulsen, D. Moia, X. Chen, S. Griggs, J. T. Mefford, R. B. Rashid, A. Marks, S. Inal, D. S. Ginger, A. Giovannitti, J. Nelson, *J. Am. Chem. Soc.* **2021**, *143*, 14795.
[74] H.-Y. Wu, C.-Y. Yang, Q. Li, N. B. Kolhe, X. Strakosas, M.-A. Stoeckel, Z. Wu, W. Jin, M. Savvakis, R. Kroon, D. Tu, H. Y. Woo, M. Berggren, S. A. Jenekhe, S. Fabiano, *Adv. Mater.* **2021**, *33*, 2106235.
[75] Y. Wang, E. Zeglio, L. Wang, S. Cong, G. Zhu, H. Liao, J. Duan, Y. Zhou, Z. Li, D. Mawad, A. Herland, W. Yue, I. McCulloch, *Adv. Funct. Mater.* **2022**, *32*, 2111439.
[76] D. Jeong, I.-Y. Jo, S. Lee, J. H. Kim, Y. Kim, D. Kim, J. R. Reynolds, M.-H. Yoon, B. J. Kim, *Adv. Funct. Mater.* **2022**, *32*, 2111950.
[77] J. Shi, P. Li, X.-Y. Deng, J. Xu, Z. Huang, Y. Lei, Y. Wang, J.-Y. Wang, X. Gu, T. Lei, *Chem. Mater.* **2022**, *34*, 864.
[78] A. Marks, X. Chen, R. Wu, R. B. Rashid, W. Jin, B. D. Paulsen, M. Moser, X. Ji, S. Griggs, D. Meli, X. Wu, H. Bristow, J. Strzalka, N. Gasparini, G. Costantini, S. Fabiano, J. Rivnay, I. McCulloch, *J. Am. Chem. Soc.* **2022**, *144*, 4642.
[79] H. Liao, J. Chen, L. Lan, Y. Yu, G. Zhu, J. Duan, X. Zhu, H. Dai, M. Xiao, Z. Li, W. Yue, I. McCulloch, *ACS Appl. Mater. Interfaces* **2022**, *14*, 16477.
[80] Y. Zhang, G. Ye, T. P. A. van der Pol, J. Dong, E. R. W. van Doremaele, I. Krauhausen, Y. Liu, P. Gkoupidenis, G. Portale, J. Song, R. C. Chiechi, Y. van de Burgt, *Adv. Funct. Mater.* **2022**, *32*, 2201593.
[81] S. Cong, J. Chen, L. Wang, L. Lan, Y. Wang, H. Dai, H. Liao, Y. Zhou, Y. Yu, J. Duan, Z. Li, I. McCulloch, W. Yue, *Adv. Funct. Mater.* **2022**, *32*, 2201821.
[82] K. Feng, W. Shan, J. Wang, J.-W. Lee, W. Yang, W. Wu, Y. Wang, B. J. Kim, X. Guo, H. Guo, *Adv. Mater.* **2022**, *34*, 2201340.
[83] J. Duan, G. Zhu, L. Wang, J. Chen, S. Cong, X. Zhu, Y. Zhou, Z. Li, I. McCulloch, W. Yue, *Adv. Funct. Mater.* **2022**, *32*, 2203937.
[84] G. Zhu, J. Chen, J. Duan, H. Liao, X. Zhu, Z. Li, I. McCulloch, W. Yue, *ACS Appl. Mater. Interfaces* **2022**, *14*, 43586.
[85] I. P. Maria, S. Griggs, R. B. Rashid, B. D. Paulsen, J. Surgailis, K. Thorley, V. N. Le, G. T. Harrison, C. Combe, R. Hallani, A. Giovannitti, A. F. Paterson, S. Inal, J. Rivnay, I.

McCulloch, *Chem. Mater.* **2022**, *34*, 8593.
[86] J. Duan, G. Zhu, L. Lan, J. Chen, X. Zhu, C. Chen, Y. Yu, H. Liao, Z. Li, I. McCulloch, W. Yue, *Angew. Chem. Int. Ed.* **2023**, *62*, e202213737.
[87] J. Chen, S. Cong, L. Wang, Y. Wang, L. Lan, C. Chen, Y. Zhou, Z. Li, I. McCulloch, W. Yue, *Mater. Horiz.* **2023**, *10*, 607.
[88] Y. Wang, G. Zhu, E. Zeglio, T. C. H. Castillo, S. Haseena, M. K. Ravva, S. Cong, J. Chen, L. Lan, Z. Li, A. Herland, I. McCulloch, S. Inal, W. Yue, *Chem. Mater.* **2023**, *35*, 405.
[89] J. Guo, L. Q. Flagg, D. K. Tran, S. E. Chen, R. Li, N. B. Kolhe, R. Giridharagopal, S. A. Jenekhe, L. J. Richter, D. S. Ginger, *J. Am. Chem. Soc.* **2023**, *145*, 1866.
[90] S. Kang, J. Fan, J. B. P. Soares, M. Gupta, *RSC Adv.* **2023**, *13*, 5096.
[91] K.-K. Liu, P. Li, Y. Lei, Z. Zhang, X. Pan, S. K. So, T. Lei, *Adv. Funct. Mater.* **2023**, *33*, 2300049.
[92] Y. Yu, G. Zhu, L. Lan, J. Chen, X. Zhu, J. Duan, S. Cong, Z. Li, Y. Wang, Z. Wang, I. McCulloch, W. Yue, *Adv. Funct. Mater.* **2023**, *33*, 2300012.
[93] J. Duan, G. Zhu, J. Chen, C. Zhang, X. Zhu, H. Liao, Z. Li, H. Hu, I. McCulloch, C. B. Nielsen, W. Yue, *Adv. Mater.* **2023**, *35*, 2300252.
[94] A. Erhardt, A. Hochgesang, C. R. McNeill, M. Thelakkat, *Adv. Electron. Mater.* **2023**, *9*, 2300026.
[95] J. Rivnay, P. Leleux, M. Ferro, M. Sessolo, A. Williamson, D. A. Koutsouras, D. Khodagholy, M. Ramuz, X. Strakosas, R. M. Owens, C. Benar, J.-M. Badier, C. Bernard, G. G. Malliaras, *Sci. Adv.* **2015**, *1*, e1400251.
[96] S. Inal, J. Rivnay, A. I. Hofmann, I. Uguz, M. Mumtaz, D. Katsigiannopoulos, C. Brochon, E. Cloutet, G. Hadziioannou, G. G. Malliaras, *J. Polym. Sci., Part B: Polym. Phys.* **2016**, *54*, 147.
[97] J. Rivnay, S. Inal, B. A. Collins, M. Sessolo, E. Stavrinidou, X. Strakosas, C. Tassone, D. M. Delongchamp, G. G. Malliaras, *Nat. Commun.* **2016**, *7*, 11287.
[98] S.-M. Kim, C.-H. Kim, Y. Kim, N. Kim, W.-J. Lee, E.-H. Lee, D. Kim, S. Park, K. Lee, J. Rivnay, M.-H. Yoon, *Nat. Commun.* **2018**, *9*, 3858.
[99] X. Wu, A. Surendran, J. Ko, O. Filonik, E. M. Herzig, P. Müller-Buschbaum, W. L. Leong, *Adv. Mater.* **2019**, *31*, 1805544.
[100] L. V. Lingstedt, M. Ghittorelli, H. Lu, D. A. Koutsouras, T. Marszalek, F. Torricelli, N. I. Crăciun, P. Gkoupidenis, P. W. M. Blom, *Adv. Electron. Mater.* **2019**, *5*, 1800804.
[101] S. Wustoni, T. C. Hidalgo, A. Hama, D. Ohayon, A. Savva, N. Wei, N. Wehbe, S. Inal, *Adv. Mater. Technol.* **2020**, *5*, 1900943.
[102] K. Tang, W. Miao, S. Guo, *ACS Appl. Polym. Mater.* **2021**, *3*, 1436.
[103] X. Wu, A. Surendran, M. Moser, S. Chen, B. T. Muhammad, I. P. Maria, I. McCulloch, W. L. Leong, *ACS Appl. Mater. Interfaces* **2020**, *12*, 20757.
[104] J. Ko, X. Wu, A. Surendran, B. T. Muhammad, W. L. Leong, *ACS Appl. Mater. Interfaces* **2020**, *12*, 33979.
[105] V. Bertana, G. Scordo, M. Parmeggiani, L. Scaltrito, S. Ferrero, M. G. Gomez, M. Cocuzza, D. Vurro, P. D'Angelo, S. Iannotta, C. F. Pirri, S. L. Marasso, *Sci. Rep.* **2020**, *10*, 13335.
[106] J. H. Kim, Z. Ahmad, Y. Kim, W. Kim, H. Ahn, J.-S. Lee, M.-H. Yoon, *Chem. Mater.* **2020**, *32*, 8606.
[107] Y. Kim, H. Noh, B. D. Paulsen, J. Kim, I.-Y. Jo, H. Ahn, J. Rivnay, M.-H. Yoon, *Adv. Mater.* **2021**, *33*, 2007550.
[108] X. Wu, M. Stephen, T. C. Hidalgo, T. Salim, J. Surgailis, A. Surendran, X. Su, T. Li, S. Inal, W. L. Leong, *Adv. Funct. Mater.* **2022**, *32*, 2108510.
[109] T. Nguyen-Dang, S. Chae, K. Harrison, L. C. Llanes, A. Yi, H. J. Kim, S. Biswas, Y.

Visell, G. C. Bazan, T.-Q. Nguyen, *ACS Appl. Mater. Interfaces* **2022**, *14*, 12469.
[110] L. Wang, Q. Sun, L. Zhang, J. Wang, G. Ren, L. Yu, K. Wang, Y. Zhu, G. Lu, H.-D. Yu, *Macromol. Rapid Commun.* **2022**, *43*, 2200212.
[111] C.-Y. Lo, Y. Wu, E. Awuyah, D. Meli, D. M. Nguyen, R. Wu, B. Xu, J. Strzalka, J. Rivnay, D. C. Martin, L. V. Kayser, *Polym. Chem.* **2022**, *13*, 2764.
[112] A. C. Tseng, T. Sakata, *ACS Appl. Mater. Interfaces* **2022**, *14*, 24729.
[113] M. Stephen, X. Wu, T. Li, T. Salim, K. Hou, S. Chen, W. L. Leong, *Mater. Horiz.* **2022**, *9*, 2408.
[114] T. Li, J. Y. Cheryl Koh, A. Moudgil, H. Cao, X. Wu, S. Chen, K. Hou, A. Surendran, M. Stephen, C. Tang, C. Wang, Q. J. Wang, C. Y. Tay, W. L. Leong, *ACS Nano* **2022**, *16*, 12049.
[115] H. Tang, Y. Liang, C. Liu, Z. Hu, Y. Deng, H. Guo, Z. Yu, A. Song, H. Zhao, D. Zhao, Y. Zhang, X. Guo, J. Pei, Y. Ma, Y. Cao, F. Huang, *Nature* **2022**, *611*, 271.
[116] J. H. Kim, M. Wieland, B. Omiecienski, Y. Kim, J. Park, G. Kim, S. Ludwigs, M.-H. Yoon, *Flex. Print. Electron.* **2022**, *7*, 044005.
[117] Y. Liang, H. Tang, C. Zhang, C. Liu, L. Lan, F. Huang, *ACS Appl. Mater. Interfaces* **2022**, *14*, 51165.
[118] G. E. Fenoy, R. Hasler, F. Quartinello, W. A. Marmisollé, C. Lorenz, O. Azzaroni, P. Bäuerle, W. Knoll, *JACS Au* **2022**, *2*, 2778.
[119] Š. Tumová, R. Malečková, L. Kubáč, J. Akrman, V. Enev, L. Kalina, E. Vojtková, M. Pešková, J. Víteček, M. Vala, M. Weiter, *Polym. J.* **2023**, DOI: 10.1038/s41428.